9-2020

Patagonian Aridification at the Onset of the Mid-Miocene Climatic Optimum

Robin B. Trayler
Boise State University

Matthew J. Kohn
Boise State University

M. Susana Bargo
Museo de La Plata

José I. Cuitiño
CENPAT-CONICET

Richard F. Kay
Duke University

See next page for additional authors

Paleoceanography and Paleoclimatology

RESEARCH ARTICLE
10.1029/2020PA003956

Special Section:
The Miocene: The Future of the Past

Patagonian Aridification at the Onset of the Mid-Miocene Climatic Optimum

Robin B. Trayler[1,2], Matthew J. Kohn[2], M. Susana Bargo[3], José I. Cuitiño[4], Richard F. Kay[5], Caroline A. E. Strömberg[6], and Sergio F. Vizcaíno[3]

[1]Department of Life and Environmental Sciences, University of California Merced, Merced, CA, USA, [2]Department of Geosciences, Boise State University, Boise, ID, USA, [3]División Paleontología de Vertebrados, Museo de La Plata, Unidades de Investigación, (CIC and CONICET), La Plata, Argentina, [4]Instituto Patagónico de Geología y Paleontología, CENPAT-CONICET, Puerto Madryn, Argentina, [5]Department of Evolutionary Anthropology, Trinity College and Division of Earth and Ocean Sciences, Nicholas School of the Environment, Duke University, Durham, NC, USA, [6]Department of Biology and Burke Museum of Natural History and Culture, University of Washington, Seattle, WA, USA

Abstract Fossil-rich sediments of the Santa Cruz Formation, Patagonia, Argentina, span the initiation of the Miocene Climatic Optimum (MCO), the most recent period of warm and wet conditions in the Cenozoic. These conditions drove the expansion of tropical and subtropical ecosystems to much higher latitudes, with the fossiliferous Santa Cruz Formation recording one of the southernmost examples. We collected new carbon and oxygen isotope compositions of herbivore tooth enamel from fossils ~17.4 to 16.4 Ma in age to investigate ecological and climatic changes across the initiation of the MCO. Enamel $\delta^{13}C$ values are consistent with a C_3-dominated ecosystem with moderate precipitation and a mix of wooded and more open areas. Serially sampled teeth reveal little zoning in $\delta^{13}C$ and $\delta^{18}O$ values, suggesting little seasonal variation in water and plant isotope compositions or seasonal changes in diet. Carbon isotope-based estimates of mean annual precipitation (MAP) are consistent with aridification, with MAP decreasing from ~1,000 ± 235 mm/yr at 17.4 Ma to ~525 ± 105 mm/yr at the start of the climatic optimum (~16.9 Ma). This decrease corresponds to increasing global temperatures, as indicated by marine proxy records, and was followed by a rebound to ~840 ± 270 mm/yr by ~16.4 Ma. In comparison to a modern mean annual temperature (MAT) in the region of ~8°C, oxygen isotopes indicate high MAT (at least 20°C) at the onset of the MCO at 16.9 Ma and a significant increase in MAT to ~25°C by 16.4 Ma.

Key Points:
- The Miocene Climatic Optimum interrupted a trend toward arid conditions in Patagonia
- Stable isotope-based estimates of precipitation and temperature significantly changed at the onset of the MCO
- General circulation models underestimate temperature for Miocene Patagonia

Supporting Information:
- Supporting Information S1

Correspondence to:
R. B. Trayler,
rtrayler@ucmerced.edu

Citation:
Trayler, R. B., Kohn, M. J., Bargo, M. S., Cuitiño, J. I., Kay, R. F., Strömberg, C. A. E., & Vizcaínos, S. F. (2020). Patagonian aridification at the onset of the mid-Miocene Climatic Optimum. *Paleoceanography and Paleoclimatology*, *35*, e2020PA003956. https://doi.org/10.1029/2020PA003956

Received 8 OCT 2019
Accepted 3 AUG 2020
Accepted article online 13 AUG 2020

1. Introduction

The Miocene Climatic Optimum (MCO; between approximately 17 and 14 Ma) was the warmest period of the Neogene and one of the warmest of the Cenozoic, temporarily reversing a long-term global cooling trend that began in the early Eocene (Zachos et al., 2001). Terrestrial estimates of atmospheric CO_2 concentrations are generally high (Beerling & Royer, 2011): Paleosols and stomatal density imply values of 400–800 ppm (Kürschner et al., 2008; Retallack, 2009). While some marine carbon isotope records originally suggested somewhat lower concentrations of 200–300 ppm (Pagani et al., 1999, 2005), more recent high-resolution boron isotope records from foraminifera indicate that low (~200 ppm) CO_2 concentrations at the onset of the MCO (~17 Ma) were succeeded by 100 ka oscillations between 300 and 600 ppm until 15.5 Ma (Greenop et al., 2014). General circulation models require high CO_2 concentrations of at least 300–600 ppm to accurately reproduce MCO temperature and precipitation conditions suggested by other proxy records (Henrot et al., 2010; Tong et al., 2009; You et al., 2009). Importantly, most estimated MCO CO_2 concentrations are similar to those projected over the coming century (IPCC, 2014), making the MCO an important analog for future climates.

These inferred, high atmospheric CO_2 concentrations during the MCO are thought to have driven important ecological and climatic changes. High-resolution $\delta^{18}O$ records from benthic foraminifera in the equatorial Pacific suggest abrupt global warming at the onset of the MCO (~17 Ma; Holbourn et al., 2015). Facies analysis of the AND-2A drill core suggests the East Antarctic Ice Sheet was retreating inland by ~17.1 Ma (Hauptvogel & Passchier, 2012) and reached a minimum extent during the MCO at 16.5–16.3 Ma (Passchier et al., 2011). Marine $\delta^{18}O$ records and climate modeling further suggest the East Antarctic Ice Sheet decreased to a size similar to today's as sea surface temperatures increased (Cramer et al., 2011;

Flower & Kennett, 1993, 1994; Gasson et al., 2016; Pekar & Christie-Blick, 2008; Pekar & DeConto, 2006; Sangiorgi et al., 2018; Shevenell et al., 2004). A long-term increase in marine $\delta^{13}C$ values beginning at ~16.9 Ma may reflect increased burial of organic carbon, likely tied to enhanced marine and terrestrial primary productivity (Föllmi et al., 2005). Decreasing ice volume and increasing sea surface temperatures inferred from general circulation models and marine records are interpreted to have reduced the meridional temperature gradient (Herold et al., 2010; Sangiorgi et al., 2018).

Terrestrial records provide further insights into mid-Miocene temperatures and precipitation. Floras and faunas dependent on warm, wet conditions expanded to higher latitudes in North America, South America, and Europe, reflecting coupled increases in temperature and precipitation (Böhme, 2003; Hinojosa & Villagrán, 2005; Wolfe, 1985, 1994). For example, a rise in terrestrial pollen and freshwater algae abundances in the AND-2A sediment core suggests that Miocene Antarctica warmed during the MCO, with summer temperatures of ~10°C (Warny et al., 2009). Likewise, leaf wax hydrogen isotope compositions (δD) indicate that Antarctic summer temperatures were at least 11°C warmer than today (Feakins et al., 2012). Ecometric and taxonomic analyses of palaeofloras point to the expansion of diverse forest vegetation at middle to high latitudes in North and South America (Barreda & Palazzesi, 2007; Dunn et al., 2015; Palazzesi & Barreda, 2012; Palazzesi et al., 2014; Wolfe, 1994). Similarly, leaf physiognomy and floral compositions from New Zealand suggest subtropical conditions during the MCO (MAT = 16.5–20°C; MAP = 1,500–2,500 mm/yr), capable of sustaining dense forests (Reichgelt et al., 2015).

Over the past ~130 years, the late-Early to Middle Miocene Santa Cruz Formation of Argentina (47–52°S latitude; Figure 1) has produced a wealth of terrestrial vertebrate fossils (see reviews of Vizcaíno et al., 2010, 2012a). The fauna is remarkable for both its diversity and preservation. Articulated skeletons are common, species richness is similar to modern lowland tropical forests, and marsupials, rodents, xenarthrans, primates, and a variety of ungulates are well represented (Croft, 2013; Vizcaíno et al., 2012a). The fauna and associated flora include several taxa inferred to be adapted to warm humid conditions (Brea et al., 2012; Fernicola & Albino, 2012; Kay, Perry, et al., 2012; Kay, Vizcaino, et al., 2012) and are thought to reflect MCO-driven expansions of low-latitude to midlatitude ecosystems to high latitudes (Catena & Croft, 2020; Kay, Vizcaino, et al., 2012; Spradley et al., 2019; Vizcaíno et al., 2010, 2012b). Many Santa Cruz Formation localities have been precisely dated to between 16 and 18 Ma (Fleagle et al., 1995, 2012; Perkins et al., 2012; Trayler et al., 2020), making the fauna ideal for investigating changes to Patagonian physical climate conditions (precipitation and temperature) at the onset of the MCO.

While previous examinations of Santa Cruz Formation ecology and climate have integrated several lines of floral, faunal, and sedimentological evidence (Croft, 2001; Kay, Vizcaino, et al., 2012; Raigemborn et al., 2015, 2018; Vizcaíno et al., 2010), these estimates either lump observations over the entire formation or focus on a narrow stratigraphic, and therefore temporal, range. In this study, we present new stable carbon ($\delta^{13}C$) and oxygen ($\delta^{18}O$) isotope compositions from fossil bone and tooth enamel recovered from Santa Cruz Formation strata spanning about 1 million years at the initiation of the MCO (ca. 17.4–16.5 Ma; Trayler et al., 2020). We use these data to address three questions:

1. How did high atmospheric CO_2 concentrations at the onset of the MCO affect the physical climate conditions of the Santa Cruz Formation? We use our stable isotope data coupled with existing geochronology to create a model of mean annual precipitation (MAP) and mean annual temperature (MAT) from ca. 17.4 to 16.5 Ma. We also use intratooth isotopic zoning to investigate whether and how much seasonality changed through this interval.
2. Did changing physical conditions affect the ecology of large-bodied Santa Cruz Formation ungulates? This might be expected if changes in precipitation and temperature were sufficient to alter habitat type (e.g., more or less forested conditions).
3. How well do existing general circulation models predict physical conditions for Early Miocene Patagonia? Models of MCO conditions predict a high MAP (>1,000 mm/yr) and a low MAT (5–10°C) (Henrot et al., 2010; Herold et al., 2010, 2011; Tong et al., 2009). These models rely on proxy records to both inform model construction and validate model results. Until recently, the majority of suitable terrestrial MCO proxy sites were in the Northern Hemisphere (Herold et al., 2011). Our data add to a growing body of work on Southern Hemisphere paleoclimate (e.g., Butzin et al., 2011; Feakins et al., 2012; Gasson

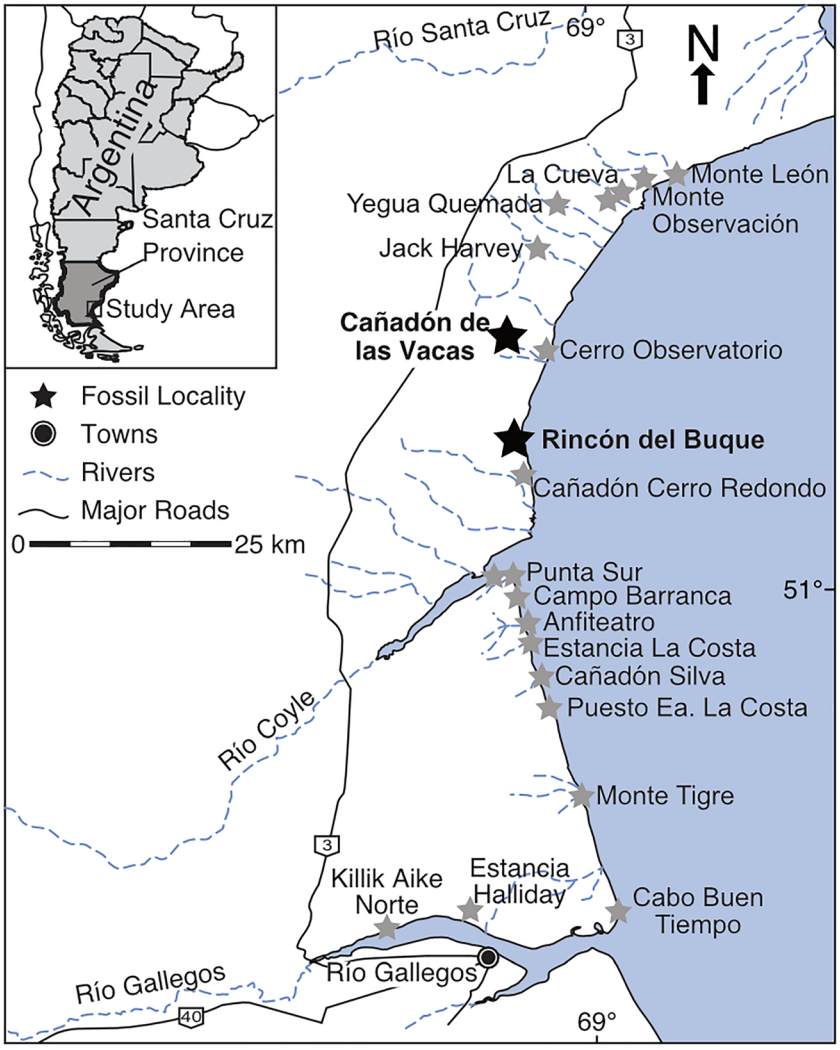

Figure 1. Map showing regional geography and Santa Cruz Formation fossil localities (modified from Vizcaíno et al., 2012a). Bold localities are included in this study.

et al., 2016; Hauptvogel & Passchier, 2012; Reichgelt et al., 2015; Sangiorgi et al., 2018; Warny et al., 2009) and add new controls on Patagonian climate during the MCO.

2. Background

2.1. Miocene Climate of Patagonia

Previously published data indicate that the Miocene climate of Patagonia was characterized by warm and moist conditions. Tropical mammals diversified and expanded south during the Early Miocene (Pascual & Ortiz Jaureguizar, 1990). Patagonia, which had been dominated by a mixture of drier lowlands interspersed with forested riparian areas, saw a southward expansion of megathermal forests reliant on high temperatures (MAT > 24°C; Barreda & Palazzesi, 2007; Dunn et al., 2015; Strömberg et al., 2013). This more closed vegetation continued to dominate the region through at least the Middle Miocene followed by cooling and aridification in the Late Miocene (Barreda & Palazzesi, 2007).

2.2. Santa Cruz Formation Paleoclimate and Paleoecology

Santa Cruz Formation exposures are extensive in southern Patagonia from the Andean foothills to the Atlantic coast (Blisniuk et al., 2005; Cuitiño & Scasso, 2010; Cuitiño et al., 2015, 2016; Fernicola et al., 2019; Marshall, 1976; Tauber, 1994, 1997a; Vizcaíno et al., 2012b). Coastal outcrops are composed primarily of

mudstones, fine- and medium-grained volcaniclastic sandstones, and numerous tuffs (Bown & Fleagle, 1993; Matheos & Raigemborn, 2012; Raigemborn et al., 2018; Tauber, 1997a). The lowest coastal exposures are consistent with a transitional continental-marine environment. The formation coarsens upward with silty sandstones and weakly-formed paleosols becoming more common, suggesting a combination of a low-energy fluvial system and floodplain deposits. The upper Santa Cruz Formation is coarser, indicating a more energetic fluvial system (Matheos & Raigemborn, 2012).

Modern conditions in our study area (Figure 1) are cool (MAT ~8°C) and semiarid (MAP ~250 mm/yr; Vizcaíno et al., 2012a), in contrast to warmer and wetter conditions for late Early Miocene that others have inferred for Patagonia and that we discuss next. Previous work on floras from the lower Santa Cruz Formation indicates a mixture of semiarid temperate forests and humid dense forests (Brea et al., 2012, 2017). Fossil wood physiognomy suggests a MAT of either 9.3 ± 1.7°C or 19.3 ± 1.7°C (Brea et al., 2012), an imprecise MAP estimate (869 ± 940 mm/yr), and a long (~7 months) dry season (Brea et al., 2012). Clay mineralogy, paleosol type, and plant macrofossils in the lower part of our section have been interpreted to indicate a warm, subhumid environment with marked seasonality (Matheos & Raigemborn, 2012; Raigemborn et al., 2018). Coarse sandstones and conglomerates are very rare, and nearly all strata point to low-flow river systems (Matheos & Raigemborn, 2012).

Mammalian faunas from the Santa Cruz Formation also suggest a complex mosaic of coexisting habitat types. Several species of arid-adapted armadillos are common (Vizcaíno et al., 2006), while glyptodonts, arboreal and terrestrial sloths, and anteaters indicate woodland and forested environments (Bargo et al., 2012). Large ungulates are also commonly recovered. The hypsodont notoungulates (*Nesodon* and *Adinotherium*) have typically been reconstructed as mixed browser-grazers or grazers, although more recent morphological (Cassini, 2013; Cassini & Vizcaíno, 2012; Cassini et al., 2012) and microwear (Townsend & Croft, 2008) analysis points to a browsing diet, consistent with the presence of some woody vegetation. Croft (2001) used cenogram analysis (ranked plots of mammalian body mass) to compare the Santa Cruz Formation to 16 modern South American faunas and concluded the fauna was characteristic of a heavily forested, wet environment (but see a critique of cenogram analyses by Kay, Vizcaino, et al., 2012). Alternatively, based on inferences of terrestrial productivity reconstructed from calculations of population densities and herbivore on-crop biomass, Vizcaíno et al. (2010) interpreted the paleoenvironment as a temperate forest and bushland, with MAP < 1,000 mm/yr. In contrast, Kay, Vizcaino, et al. (2012) reviewed existing floral and faunal constraints and using mammalian niche metrics inferred mixed forest-grasslands with MAP > 1,000 mm/yr and MAT > 14°C. Spradley et al. (2019) applied a variety of machine learning techniques to data for a variety of niche metrics (similar to those reported in Kay, Vizcaino, et al., 2012). As calibrated with modern South America, they inferred a MAP of between 850 and 1,350 mm/yr and MAT of 15–23°C for the lower Santa Cruz Formation. Recent ecological diversity analyses of the Santa Cruz fauna produced somewhat contradictory interpretations, linking the Santa Cruz fauna to Palearctic, Neoptropical, and Indo-Malayan faunas, but overall pointed to a "subtropical, mixed forest environment" (Catena & Croft, 2020) with a MAP of 1,210 to 1,286 mm/yr at the upper end of estimates (Kay, Vizcaino, et al., 2012; Spradley et al., 2019).

2.3. Stable Isotopes in Enamel and Bone

Chemically, bone and tooth enamel are composed of hydroxylapatite [$Ca_5(PO_4)_3OH$], with carbonate (CO_3) substitution in the PO_4 and OH sites (Elliott, 2002). While bone carbonate is easily altered diagenetically at ambient temperatures (Kohn & Law, 2006), enamel is resistant to alteration, retaining its primary isotope composition (Kohn & Cerling, 2002).

Tooth enamel mineralizes progressively from the occlusal (wear) surface toward the root and is not remodeled after formation. Mineralization occurs as a two-stage process—apposition and maturation (Robinson et al., 1978, 1979; Suga, 1982)—although only second stage maturation controls isotope compositions (Trayler & Kohn, 2017). Mineralization rates for ungulates vary but are commonly on the order of 40–60 mm/yr (Fricke et al., 1998; Kohn, 2004). An animal's $\delta^{18}O$ value tracks variations in the composition of meteoric water throughout the year, typically with lower values in winter and higher values in summer. Similarly, an animal's $\delta^{13}C$ value tracks variations in diet.

Changes in an animal's $\delta^{18}O$ and $\delta^{13}C$ values correlate with changes in its environment and diet and are archived in tooth enamel; however, a damping effect related to the rate of mineralization and the carbon and oxygen turnover rates in the animal reduces the overall variability of enamel isotope compositions relative to environmental variability (Kohn, 1996; Kohn et al., 1996, 1998; Passey & Cerling, 2002; Podlesak et al., 2008). That is, the total range of $\delta^{18}O$ and $\delta^{13}C$ values within a single tooth will be lower than the seasonal range of local water $\delta^{18}O$ values and plant $\delta^{13}C$ values. A variety of models have been proposed to calculate the magnitude of this damping (Green et al., 2018; Passey & Cerling, 2002; Passey, Cerling, et al., 2005; Zazzo, Lécuyer, Sheppard, et al., 2004), but in the context of improved understanding of isotopic systematics during tooth enamel mineralization (Trayler & Kohn, 2017), damping should be no more than ~50% of the total seasonal range (Kohn, 2004). Indeed, many mammalian teeth preserve isotopic seasonality in their enamel (e.g., Balasse, 2003; Balasse et al., 2012; Fricke & O'Neil, 1996; Fricke et al., 1998; Green et al., 2018; Kohn et al., 1998; Zazzo et al., 2005). Therefore, while teeth do not record the full environmental range of isotope compositions over a period of tooth growth, isotopic zoning within enamel does reflect changes in seasonality and diet. As a corollary, high versus low amplitude zoning reflects high versus low isotopic variation in the sources of oxygen and carbon that an animal ingests.

The oxygen isotope composition of tooth enamel is controlled by the composition of ingested water (Kohn, 1996; Kohn et al., 1996; Luz & Kolodny, 1985). Many large herbivores ingest much of their water via drinking, and enamel $\delta^{18}O$ values from most modern mammals strongly correlate with local water $\delta^{18}O$ values, represented by either local streams and small water bodies or amount weighted precipitation (Hoppe, 2006; Kohn, 1996; Kohn & Dettman, 2007; Kohn et al., 1996, 1998). Some drought-tolerant taxa exhibit important isotopic shifts related to aridity (Ayliffe & Chivas, 1990; Levin et al., 2006; Luz et al., 1990).

The carbon isotope composition of enamel is controlled by diet. In herbivores, enamel $\delta^{13}C$ values reflect the plants they eat plus an enrichment factor. Studies of wild and captive herbivores suggest enrichments of + 13.3–14.6‰ (Passey, Robinson, et al., 2005). Protein-based phylogenetic analyses place many South American ungulates in a monophyletic clade with nonruminant perissodactyls (Buckley, 2015; Welker et al., 2015). Likewise, morphological similarities between perissodactyls and notoungulates suggest a common hindgut fermentation strategy (Cassini et al., 2012). Harris et al. (2020) compiled data from the literature for equids and recommend a weighted average enrichment factor (ε) of 14.5‰, which we use for all enamel-diet corrections.

All plants use one of three photosynthetic pathways (C_3, C_4, or CAM) to fix atmospheric CO_2, each resulting in characteristic carbon isotope compositions. C_4 plants (modern $\delta^{13}C = -12.1 \pm 1.1$‰) are primarily warm growing season grasses, sedges, and several lineages of dicots (Sage et al., 2011). C_4 plants became a significant portion of global vegetation biomass only in the Late Miocene and Early Pliocene (Cerling et al., 1997; Edwards et al., 2010) and are therefore unlikely to have contributed significantly to the diet of Santa Cruz Formation herbivores. Likewise, CAM plants, which rarely make up a significant portion of large herbivore diets today, appear to have been neither diverse nor abundant in ecosystems prior to the Late Miocene (Edwards & Ogburn, 2012).

C_3 plants (trees, shrubs, herbs, and cool-season grasses) therefore make up the majority of both modern and late-Early Middle Miocene vegetation biomass (Cerling et al., 1997; Still et al., 2003). Modern C_3 $\delta^{13}C$ values have a mean of −28.5‰ and range from −23 to −32‰, although values more positive than −24‰ are rare (Kohn, 2010). As mid-Miocene atmospheric CO_2 $\delta^{13}C$ values were ~2.5‰ higher than modern values (Tipple et al., 2010), tooth enamel $\delta^{13}C$ values lower than ~ −7‰ (as an approximation, ~ −24‰ + 14.5‰ + 2.5‰) should reflect a diet of pure C_3 plants. $\delta^{13}C$ values in closed canopy forests are extremely low (less than ~ −31‰) due to recycling of low $\delta^{13}C$ CO_2 and low light levels in the understory (van der Merwe & Medina, 1991). Consequently, $\delta^{13}C$ values in mid-Miocene tooth enamel lower than ~ −14‰ (~ −31‰ + 14.5‰ + 2.5‰) would indicate closed-canopy forests.

3. Materials and Methods

3.1. Fossil Collection and Sampling

Fossil teeth and bone fragments from large mammals were collected in situ from two Santa Cruz Formation localities, Cañadón de las Vacas and Rincón del Buque (Figure 1). The stratigraphic position of each

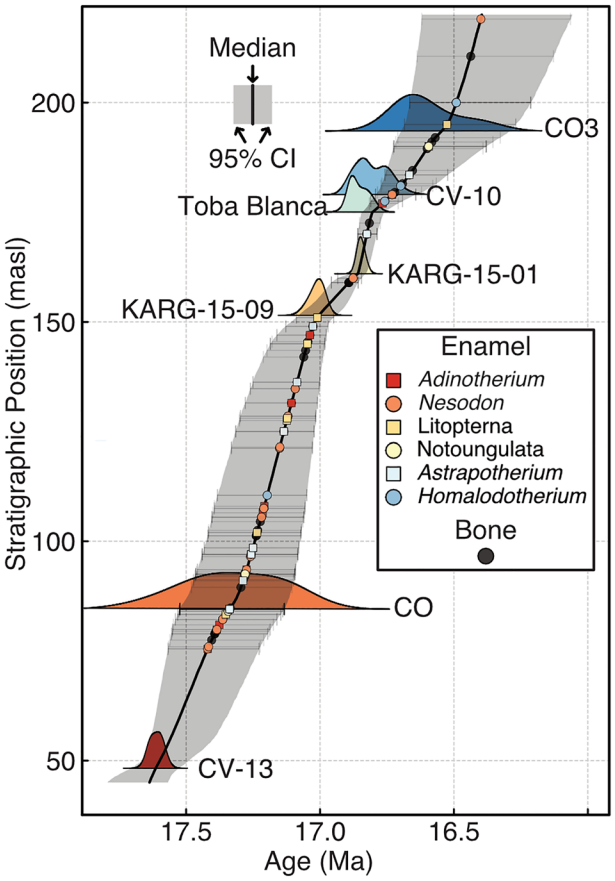

Figure 2. Age-depth model for a composite section of the Cañadón de las Vacas and Rincón del Buque localities. Colored areas with tails are the probability distribution functions for each marker tuff (modified from Trayler et al., 2020). Colored dots and error bars indicate the median age and uncertainty expressed as 95% credible intervals (CI) of fossil bone and enamel samples. See supporting information for precise stratigraphic positions for all fossil samples.

specimen was measured using a Jacob's staff relative to one of several marker tuffs of known position and age (Figure 2, supporting information). Fossil teeth are accessioned in the Museo Regional Provincial P.M.J. Molina (MPM-PV) of Río Gallegos, Santa Cruz Province, Argentina. Bone fragments were destroyed during analysis and were not accessioned. In most cases, teeth were identified to the genus level. We selected bone fragments based on their potential for isotopic analysis and made no attempt to identify them. When collecting fossil teeth, we primarily targeted large ungulates for two reasons. First, these animals are abundant throughout the section, making it possible to track the same genera through time. Assuming animals did not change the types of plants they consumed appreciably through time, changes in plant isotopic values (as opposed to differences in diet) can be assessed throughout the section. Second, large herbivores consume large amounts of plant biomass and are often less selective in their feeding than smaller animals, effectively integrating plant compositions across a large landscape into single enamel samples (Kohn, 2016).

The average sedimentation rate through our section was roughly 150 m/Ma, or 6–7 ka per meter. Thus, two laterally separated fossils collected from a typical meter-thick horizon cannot be correlated more precisely in time to better than a few thousand years. With the exception of some particularly fossiliferous levels near the base of our section (~84.5 m above sea level), we did not find fossil teeth of all taxa of interest in most stratigraphic horizons (Figure 2). However, there are no systematic increases or decreases in the abundance of one taxon relative to others through the section, such that taxonomic changes throughout the section should not drive isotopic shifts.

We sampled teeth from three orders, Notoungulata, Astrapotheria, and Litopterna. Notoungulata is represented in our sample by two families, Toxodontidae (genera: *Nesodon* and *Adinotherium*) and Homalodotheriidae (genus: *Homalodotherium*). Order Astrapotheria is represented by one family (Astrapotheriidae) and one genus (*Astrapotherium*). At least five genera within order Litopterna have been described from the Santa Cruz Formation (Cassini et al., 2012). However, our litoptern teeth were usually fragmented and were identifiable only to order Litopterna. We separately compared $\Delta^{13}C$ and $\delta^{18}O$ values (Equation 2) among taxonomic groups using analysis of variance (ANOVA) and post hoc pairwise *t* tests (with Bonferroni correction) to assess dietary similarities among taxa (Table 2). Several fragmentary teeth were identified only as "Toxodontidae indet." These samples were excluded from statistical tests, as they represent an unknown mixture of several groups, but were included in later temperature and precipitation modeling.

All teeth were lightly abraded with a carbide burr to remove surficial material before sampling. About 10 mg of enamel powder was collected from each tooth using a 0.5 mm inverted cone carbide dental drill bit and a Dremel® rotary tool. To characterize broad isotopic trends, we collected bulk enamel samples by drilling a

Table 2
Statistical Comparisons of $\delta^{18}O$ Values for Santa Cruz Formation Herbivores

Taxa	*Astrapotherium*	*Homalodotherium*	*Litopterna*	*Nesodon*
Adinotherium	S	NS	S	NS
Astrapotherium	—	S	S	S
Homalodotherium	—	—	NS	NS
Litopterna	—	—	—	S

Note. NS, no significant difference ($p > 0.05$); S, significant differences ($p < 0.05$).

single continuous groove parallel to the growth axis for the entire length of the available enamel. In most cases, this process averaged several cm of enamel into a single sample, effectively integrating a large portion of (possible) isotopic seasonality. To characterize seasonality, we also collected serial samples from a subset of teeth to examine intratooth isotopic zoning. Five molars were subsampled in detail along the tooth and perpendicular to the growth axis—one *Astrapotherium*, one *Homalodotherium*, and three *Nesodon*.

Each bone analysis represents a composite of several ($n > 5$) laterally separated bone fragments from the same horizon. These fragments were sonicated in deionized water to remove surficial material and ground independently in a mortar. Equal volumes of each resulting powder were mixed.

After sampling, we pretreated all enamel and bone powders following the procedures of Koch et al. (1997) to remove organic contaminants and labile carbonates. The isotope composition of the carbonate component of each sample was measured by phosphoric acid digestion at 70°C using a 2010 ThermoFisher GasBench II coupled with a Delta V+ continuous flow isotope ratio mass spectrometer located in the Stable Isotope Laboratory, Department of Geosciences, Boise State University. All stable isotope analyses in this study are from the carbonate component and are reported in the standard delta notation relative to VPDB and VSMOW for $\delta^{13}C$ and $\delta^{18}O$, respectively. All analyses were standardized to VPDB ($\delta^{13}C$) and VSMOW ($\delta^{18}O$) using the NBS-18 and NBS-19 calcite standard reference materials. Analytical reproducibility for both standards was ±0.1–0.2 ($n = 46$; 2σ) for both $\delta^{13}C$ and $\delta^{18}O$. We also analyzed several replicates of NIST 120c, a phosphorite with chemistry similar to enamel and bone, as a preparation standard. Average compositions for NIST120c were −6.52 ± 0.14‰ ($n = 20$; 2σ) and 28.89 ± 0.65‰ ($n = 20$; 2σ) for $\delta^{13}C$ and $\delta^{18}O$, respectively.

3.2. Precipitation Estimations

C_3 plant $\delta^{13}C$ values are sensitive to aridity, with $\delta^{13}C$ values decreasing with increased water availability (Diefendorf et al., 2010; Ehleringer, 1989; Ehleringer & Cooper, 1988; Farquhar et al., 1989; Kohn, 2010). This relationship allows very broad inference of habitat type, with higher $\delta^{13}C$ values associated with open habitats (savanna and scrublands) and lower values associated with closed habitats (forests). The dependency of the carbon isotope compositions of C_3 plants on water availability also allows MAP to be calculated from enamel $\delta^{13}C$ values:

$$\mathrm{MAP} = 10^{\left[\frac{\Delta^{13}C - 2.01 + 0.000198 \times \mathrm{elevation} - 0.0129 \times \mathrm{abs(latitude)}}{5.88}\right]} - 300 \quad (1)$$

where elevation and latitude are in meters and degrees (Kohn, 2010). $\Delta^{13}C$ is given by

$$\Delta^{13}C = \frac{\delta^{13}C_{atm} - \left(\delta^{13}C_{leaf}\right)}{1 + \left(\delta^{13}C_{leaf}\right)/1,000} \quad (2)$$

which corrects $\delta^{13}C_{leaf}$ values for changes to atmospheric CO_2 $\delta^{13}C$ values. $\delta^{13}C_{leaf}$ is calculated using our measured herbivore enamel carbon isotope compositions and a nonruminant specific enrichment factor:

$$\delta^{13}C_{leaf} = \frac{\delta^{13}C_{enamel} - 14.5}{1 + \frac{14.5}{1,000}} \quad (3)$$

Whereas South America has moved westward since the Miocene (Hartnady & Le Roex, 1985), there have been changes of less than 5° in latitude and negligible changes in elevation in the study area; we therefore use a modern elevation of ~20 m and latitude of −50.5° for all specimens. Even so, regression coefficients in Equation 1 show that these two parameters have little overall effect on MAP calculations.

We used the approach of Tipple et al. (2010) to calculate $\delta^{13}C_{atm}$ from the high-resolution benthic foraminifera records of Holbourn et al. (2015). We made no corrections to our data for changes in atmospheric CO_2 concentrations. While weeks- to months-long controlled experiments imply a dependency between C_3 plant $\delta^{13}C$ values and atmospheric CO_2 concentrations (Schubert & Jahren, 2012), modern and fossil tooth enamel proxy records do not resolve a dependence of plant $\delta^{13}C$ values on atmospheric CO_2 concentrations (Kohn, 2016).

3.3. Temperature Estimations

Bone is mineralogically similar to enamel but has a proportionally higher carbonate content in the apatite structure (Driessens & Verbeeck, 1990) and is more finely crystalline, increasing its susceptibility to chemical alteration and recrystallization during fossilization (Ayliffe et al., 1994; Trueman & Tuross, 2002). Isotopic resetting of the carbonate component of bone apatite is thought to occur during fossilization at ambient soil temperatures in equilibrium with soil water oxygen isotope compositions (Kohn & Law, 2006). Because fossilization and recrystallization occur over a few tens of thousands of years (Kohn & Law, 2006) and accumulation rates for the localities studied here were ~0.15 m/ka (Perkins et al., 2012; Trayler et al., 2020), most fossilization and isotopic resetting likely occurred at a depth of ≥1 m below the surface, limiting evaporative enrichment of soil water. Consequently, we assume that soil water compositions mirror local water compositions, although the two sources are not necessarily the same physical water. We also assume that soil temperatures reflect MAT. Soil temperatures correlate well with air temperatures at a depth of a few centimeters to a few meters. At shallow depths (<1 m), soil temperatures may be higher than air temperatures, while at greater depths, soil temperatures do not appear to differ significantly from MAT (Paul et al., 2004; West, 1952; Zheng et al., 1993).

Given an independent record of local water $\delta^{18}O$ values (enamel) and the temperature dependence of $CaCO_3$-water oxygen isotope fractionation (Kim & O'Neil, 1997), bone and enamel oxygen isotope compositions can be related to temperature (Zanazzi et al., 2007):

$$\mathrm{MAT}\ (^{\circ}\mathrm{C}) = \frac{18,030}{1000\ln\left(\dfrac{1+\dfrac{\left(\delta^{18}O_{\mathrm{bone}} - 2.2 \pm 0.6\right)}{1,000}}{1+\dfrac{\left(1.15 \pm 0.08 \times \delta^{18}O_{\mathrm{enamel}} - 36.3 \pm 1.6\right)}{1,000}}\right) + 32.42} - 273.15 \quad (4)$$

where $\delta^{18}O_{\mathrm{bone}}$ and $\delta^{18}O_{\mathrm{enamel}}$ are expressed in VSMOW.

We propagated model errors and uncertainties in $\delta^{18}O_{\mathrm{bone}}$ and $\delta^{18}O_{\mathrm{enamel}}$ using a Monte Carlo approach. These calculations account for temporal uncertainties and compositional scatter in the data, uncertainties in the global correlation of tooth enamel isotope composition and local water composition (denominator of the ln term, Equation 4), and the calibration uncertainty that links bone and calcite $\delta^{18}O$ (numerator of the ln term, Equation 4). Physiology can impact mammal isotope composition (Kohn, 1996), especially an animal's water dependence, and potentially bias MAT calculations. While the exact physiology of an extinct organism can never be known, notoungulates likely shared the same plesiomorphic digestive physiology (hindgut fermentation) as modern perissodactyls, as indicated from craniodental and molecular phylogenetic analysis (Buckley, 2015; Cassini et al., 2012; Fletcher et al., 2010; Kohn et al., 2015; Welker et al., 2015). Hindgut fermenters have high daily water requirements, and their $\delta^{18}O$ values group with other large water-dependent herbivores along a strong global correlation between animal $\delta^{18}O$ and local water $\delta^{18}O$. Thus, the $\delta^{18}O$ values of the large notoungulates that we analyzed should logically correlate with local water compositions in the same way that is observed today for perissodactyls and other large water-dependent animals. While we cannot quantify the uncertainty in this assumption, it seems likely to be much smaller than the scatter in modern data that is accounted for already in our error estimates.

We also cannot directly quantify errors in our assumption that soil water composition and temperature at the site of bone fossilization reflect local water composition and local MAT. However, in principle, alternative assumptions should induce systematic offsets in temperature calculations rather than changing absolute errors. For example, if soil temperatures were 2°C higher than surface air temperatures, then our MAT estimates would be 2°C too high. Taken together, our estimates of temperature uncertainty must be minima, but changes to MAT are likely to be resolved more accurately than absolute temperatures.

3.4. Age-Depth Modeling and Isotope Compositions

Based on U-Pb and $^{40}Ar/^{39}Ar$ ages of multiple dated tuffs, the age of the Cañadón de las Vacas and Rincón del Buque localities (Figure 2) is between ~17.4 and ~16.5 Ma (Perkins et al., 2012; Trayler et al., 2020). Trayler et al. (2020) also used a modified version of the Bayesian age-depth model Bchron (Haslett &

Table 1
Summary Statistics for All Taxonomic Groups

	$\delta^{13}C$		$\delta^{18}O$		
Taxa	Mean	2σ	Mean	2σ	*n*
Nesodon	−11.36	1.74	22.94	2.53	32
Adinotherium	−12.23	2.43	23.30	2.83	18
Litopterna	−11.18	2.46	24.82	4.01	11
Astrapotherium	−10.88	2.03	20.84	1.51	11
Homalodotherium	−10.62	2.37	24.44	1.80	5
Toxodontidae indet.	−11.62	2.13	23.54	2.37	8

Note. The Toxodontidae indet. group likely represents a combination of *Nesodon*, *Adinotherium*, and *Homalodotherium*.

Parnell, 2008) to construct a continuous model of age and uncertainty estimates for a composite of these two localities (Figure 2). We use this model and stratigraphic correlations between Cañadón de las Vacas and Rincón del Buque to calculate age and uncertainty for each enamel and bone sample based on its stratigraphic position relative to one or more dated tuffs. Age-depth models provide an age estimate for each stratigraphic position, with uncertainties that vary with stratigraphic distance from the dated tuffs.

Trayler et al. (2020) offer a Monte Carlo method to propagate age-depth model uncertainties onto paleoclimate proxy records while respecting the stratigraphic superposition relationships among the samples. This method involves four basic steps: (1) Use age-depth model results to estimate a set of ages for each bone and enamel sample. (2) Apply a smoothing function to the proxy data (stable isotope records) to attenuate high-frequency noise. In this case, we use a moving average, which weights all data points using a Gaussian kernel and a smoothing window size of 0.05 Ma. (3) Repeat Steps 1 and 2 many times (>10,000) and store the results. (4) Calculate summary statistics (median, 95% CI) over all smoothed isotope compositions.

We smoothed bulk enamel $\delta^{13}C$, bulk enamel $\delta^{18}O$, and bone $\delta^{18}O$ values using the Monte Carlo method outlined above (Trayler et al., 2020). We allowed the isotope composition of each sample to vary by ±1.6‰ for oxygen and ±0.6‰ for carbon to reflect intratooth variations in isotope composition (discussed below). All fossil-age predictions, statistical analysis, and data smoothing were performed using R v. 3.3.3 (R Core Team, 2019).

4. Results

4.1. Bulk Isotope Compositions

Enamel $\delta^{13}C$ values have a mean value of −11.4 ± 2.3‰ (2σ; Table 1 and Figure 3), with a maximum value of −8.8‰, consistent with a diet of purely C_3 plants. Enamel $\delta^{18}O$ values have a mean value of 23.1 ± 3.4‰. Bone $\delta^{13}C$ and $\delta^{18}O$ values are similar to those of enamel with means of −10.6 ± 3.8‰ and 21.8 ± 1.8‰, respectively. Stable isotope compositions and stratigraphic positions for all samples may be found in the supporting information (Tables S1 and S2).

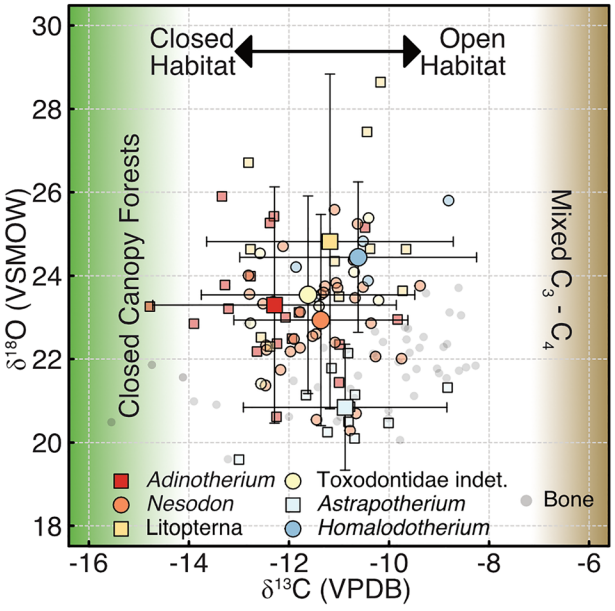

Figure 3. $\delta^{13}C$ versus $\delta^{18}O$ values for Santa Cruz Formation herbivores. Large symbols with error bars are the mean ± 2σ for each taxonomic group. Shaded areas at −15‰ and −7.5‰ indicate the transitions for closed-canopy forests (C_3) and mixed C_3-C_4 environments (see section 2.2 for details).

Although we include undifferentiated notoungulate data in later temperature and precipitation modeling calculations, we excluded these data from statistical tests as they represent a combination of *Adinotherium*, *Nesodon*, and *Homalodotherium*. Because fossil ages span ~1 Ma (discussed below), we tested the equivalence of means among taxa using $\Delta^{13}C$ values (Equation 2), which corrects for changes to the $\delta^{13}C$ of the atmosphere. *Nesodon*, *Adinotherium*, *Astrapotherium*, *Homalodotherium*, and litopterns show no significant differences in $\Delta^{13}C$ values (ANOVA; $p > 0.05$). $\delta^{18}O$ values among taxa show statistically significant differences (ANOVA; $p < 0.05$). Post hoc pairwise *t* tests (with Bonferroni correction; Table 2) reveal that *Astrapotherium* $\delta^{18}O$ values are significantly lower than all other taxa and that litoptern $\delta^{18}O$ values are significantly higher than all groups except *Homalodotherium*.

4.2. Intratooth Isotope Zoning

Zoning profiles along the five molars that we analyzed reveal low to moderate variation in carbon and oxygen isotope compositions over the length of each tooth (Figure 4 and Table S2). Although enamel mineralization rates for notoungulates and astrapotheres are unknown, rates for horses and bovids vary between 40 and 60 mm/yr (Kohn, 2004; Trayler & Kohn, 2017), suggesting that our zoning profiles should represent about

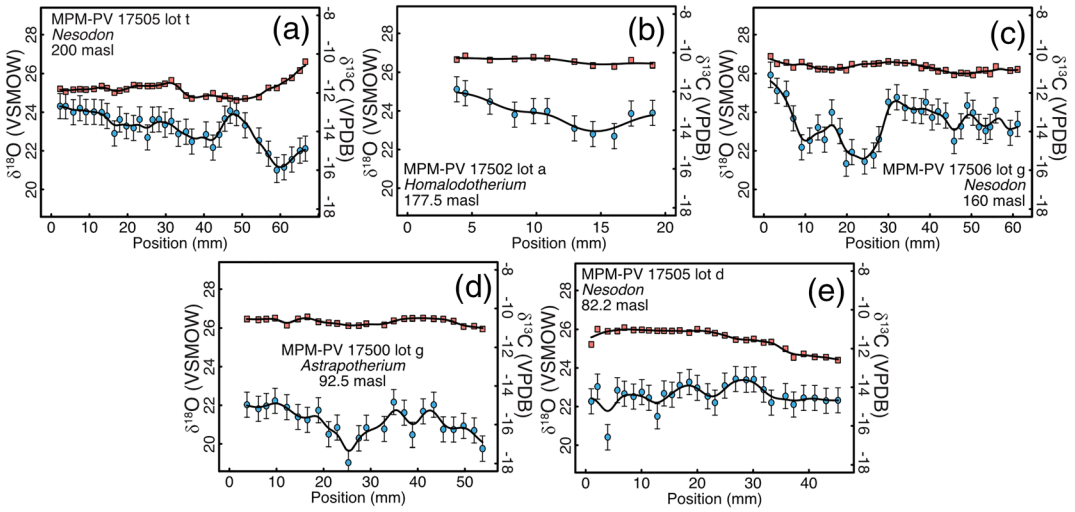

Figure 4. Carbon (squares) and oxygen (circles) isotope zoning profiles from Santa Cruz Formation ungulate tooth enamel, arranged according to stratigraphic level (top to bottom). Error bars indicate 2σ analytical reproducibility for replicates of the NIST120c reference material. Error bars for $\delta^{13}C$ values are smaller than the symbols. (a) *Nesodon*, (b) *Homalodotherium*, (c) *Nesodon*, (d) *Astrapotherium*, and (e) *Nesodon*.

~0.5 to 1.5 years of enamel growth. Overall, $\delta^{13}C$ values within a single tooth show low variance, with an average intratooth variation of ±0.6‰ (2σ). Carbon isotope compositions from one individual (CV-RT-15-016) displays an ~2‰ change in $\delta^{13}C$ values over ~20 mm, which is the maximum observed variability. $\delta^{18}O$ values show somewhat more variation, with an average intratooth variability of ±1.6‰ (2σ). Oxygen isotope zoning profiles do not reveal a clear structure; that is, there is no quasi-sinusoidal variation in $\delta^{18}O$ values that usually results from strong seasonal variations in meteoric water isotope compositions. Instead, three teeth show several millimeters of unchanged isotope compositions followed by sharp excursions toward low $\delta^{18}O$ values.

4.3. Fossil Age-Depth Modeling and Smoothing

Model ages for enamel and bone samples range from ~17.4 to ~16.4 Ma (Figure 2). Samples located near dated tuffs are best constrained temporally and have uncertainties similar to the tuffs themselves (typically ±0.03 Ma), while samples that are stratigraphically farthest from dated tuffs have the highest age uncertainties (up to ±0.28 Ma). Although sampling of individual taxa was not identical either stratigraphically (Figure 2) or temporally (Figures 5a and 5b), pairwise Kolmogorov-Smirnov tests reveal no significant differences ($p > 0.05$) in the stratigraphic distribution of taxonomic groups. That is, each taxonomic group can be thought of as a sample from the same underlying distribution of fossils. However, the sampling density of each group does vary throughout the section. *Nesodon* and *Adinotherium* are the most common and are well represented throughout. Litopterns and *Astrapotherium* are less common but are still represented over most of the section. *Homalodotherium* is the least abundant taxon, represented by only five individuals. Sampling heterogeneities are partially mitigated by two factors. First, because large herbivores consume large amounts of plant matter, they act as effective integrators of plant isotope compositions. Second, because our smoothing model allows the age of each individual data point to vary probabilistically, heterogeneities in taxa distributions are also smoothed. Last, we do not detect any significant differences in $\delta^{13}C$ values among the four taxa, so sampling of one taxon for carbon isotope compositions is plausibly indistinguishable from sampling another. Nonetheless, we also report smoothed isotope profiles for only Toxodontidae (*Nesodon* and *Adinotherium*; Figures 5 and 6), because this group makes up a majority (~60%) of our samples.

Smoothed enamel $\delta^{13}C$ values increased from −12‰ to ~ −10.5‰ between 17.4 and ~16.9 Ma, followed by a slight decrease of ~0.4‰ before remaining unchanged until the end of the record (Figure 5a). Smoothed enamel $\delta^{18}O$ values followed a similar trajectory (Figure 5b), with an increase from 23‰ to 24‰ between ~17.4 to ~16.9 Ma followed by a gradual increase of ~0.6‰ until the end of the record.

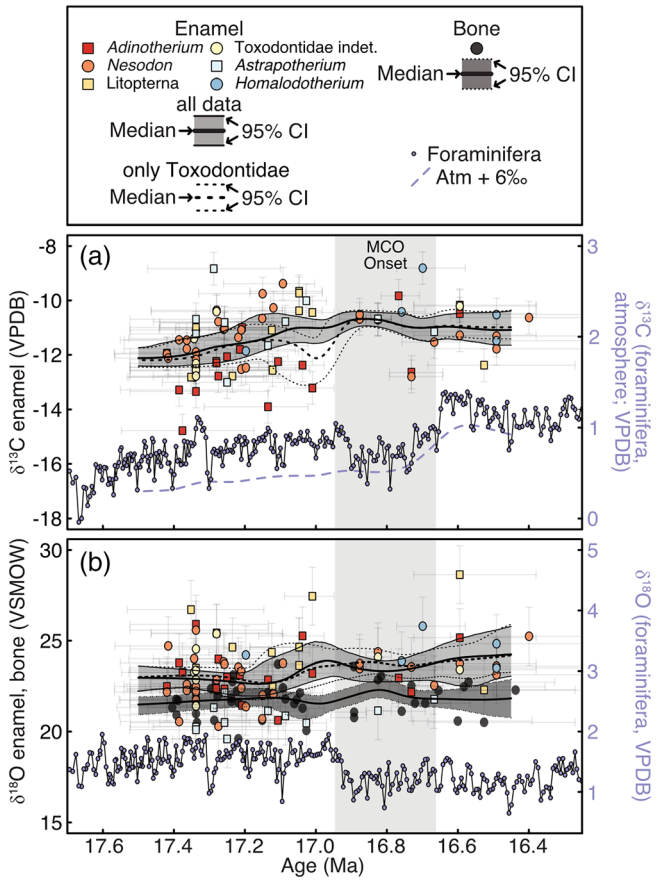

Figure 5. Plots of $\delta^{13}C$ and $\delta^{18}O$ values versus age. Solid black lines and shaded gray area are the median and 95% CI of smoothed isotope composition for all enamel data. Dashed black lines are the median and 95% CI of data from family Toxodontidae only. Small purple dots on both plots are benthic foraminifera data from Holbourn et al. (2015) for comparison. Shaded gray rectangle corresponds to rapid warming at the onset of the MCO (Holbourn et al., 2015). (a) Plot of enamel $\delta^{13}C$ values versus age. Dashed purple line is the $\delta^{13}C$ of atmospheric CO_2 (+6‰ for ease of comparison) calculated as described in section 3.2. Smooth curves for all data and for Toxodontidae-only show an increase or ~1‰ by 16.9 Ma, followed by stasis to the end of the record. (b) Plot of enamel and bone $\delta^{18}O$ values versus age. Dark gray shaded area and solid black line are the median and 95% CI of smoothed isotope composition for all bone data. Bone and enamel compositions diverge starting about 17.1 Ma and then converge by 16.8 Ma.

5. Discussion

5.1. Diagenetic Alteration

The flat, nonsinusoidal composition profiles might be viewed as a possible indicator of diagenetic alteration. However, modern ungulate teeth from Bolivia show similarly flat profiles (Bershaw et al., 2010), so flat profiles do occur in unaltered tooth enamel. Other observations are consistent with preservation of original biogenic compositions. For example, $\delta^{13}C$ values fall within ranges of a pure C_3 diet, and (as discussed in section 5.2) $\delta^{18}O$ values *Astrapotherium* are lower than for other taxa, as expected for (hypothesized) semiaquatic mammals (Clementz et al., 2008). Lastly, microbially mediated dissolution-reprecipitation of enamel apatite is viewed as the dominant driver of isotopic alteration in tooth enamel (Zazzo, Lécuyer, & Mariotti, 2004). However, the fossil teeth that we analyzed preserve exquisite biogenic textures, including decussate fibers of apatite, Hunter-Schreger bands, incremental lines, and surface polish. Microbial processes would likely eradicate these textures.

5.2. Ecology of Large-Bodied Santa Cruz Formation Ungulates

Only one enamel $\delta^{13}C$ values fall within the expected range for closed-canopy forests (−14‰), while none fall within the range of mixed C_3-C_4 environments. The lack of significant differences among herbivore $\delta^{13}C$ values suggests dietary homogeneity or resource partitioning in ways not readily distinguished using carbon isotopes (e.g., feeding at different times, feeding on different parts of a plant, and feeding on different plants with similar $\delta^{13}C$ values). Intermediate $\delta^{13}C$ values (−7 to −14‰) are usually interpreted as open woodlands or mixed woodland-scrubland environments (Feranec & MacFadden, 2006; Kohn et al., 2005; Trayler et al., 2015). Given the range of observed $\delta^{13}C$ values, all sampled herbivores were likely mixed feeders or browsers, moving between wooded and open areas but not occupying closed-canopy systems.

Homalodotherium limb morphology indicates the ability to adopt a bipedal posture, freeing the forelimbs and enabling browsing in the lower canopy (Cassini et al., 2012; Elissamburu, 2010). Morphofunctional and morphometric analysis of skulls has variously proposed a grazing or mixed feeding niche for the notoungulates *Nesodon* and *Adinotherium* (Cassini, 2013; Cassini & Vizcaíno, 2012; Cassini et al., 2012), while enamel microwear suggests a primarily browsing diet for both taxa (Townsend & Croft, 2008). *Adinotherium* has the lowest observed $\delta^{13}C$ values, but mean *Nesodon* $\delta^{13}C$ values are only slightly higher than for *Adinotherium*. Given the similarity among $\delta^{13}C$ values of *Homalodotherium*, *Nesodon*, and *Adinotherium*, our isotopic data are compatible with a browsing diet for all these taxa. Similarly, our data support the interpretation of brachydont litopterns as browsers (Cassini, 2013; Cassini & Vizcaíno, 2012; Cassini et al., 2012). However, since the carbon isotope composition for C_3 grasses (−26.7 ± 2.3‰; Cerling et al., 1997) falls in the middle of the overall range in C_3 plants ($\delta^{13}C$ ~ −23 to −32‰), we cannot exclude the possibility of C_3 grazing.

While *Astrapotherium* $\delta^{13}C$ values do not differ significantly from other taxa, its mean $\delta^{18}O$ value is ~2.5‰ lower than the mean for all other taxa. Analysis of limb morphology led Avilla and Vizcaíno (2005) to conclude that *Astrapotherium* was semiaquatic, while Cassini et al. (2012) proposed that its limbs resembled those of the Indian Rhinoceros (*Rhinoceros unicornis*), which commonly wallows and browses in lakes and rivers (Laurie et al., 1983). Increased water availability can allow rapid turnover of body water, which drives $\delta^{18}O$ values (lower) toward local water $\delta^{18}O$ (Clementz et al., 2008; Kohn, 1996; MacFadden, 1998).

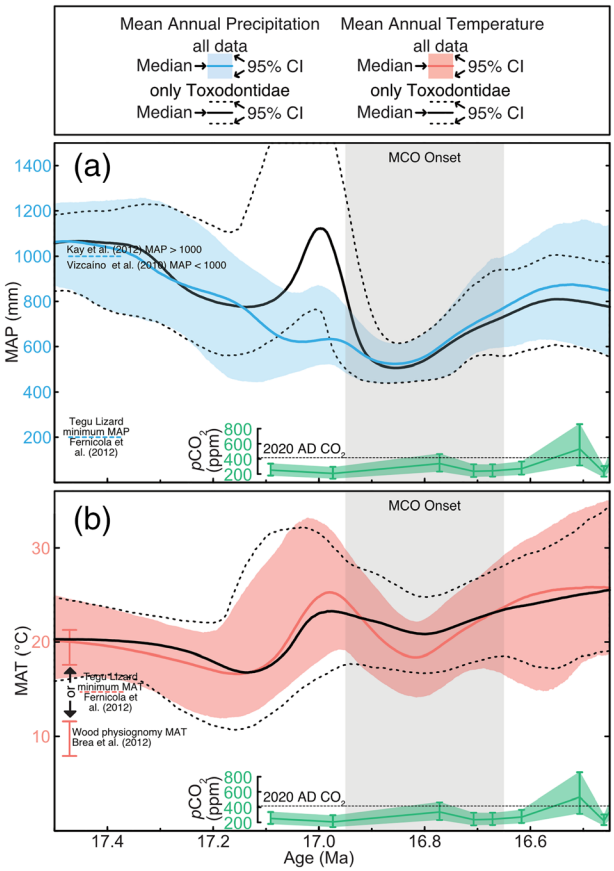

Figure 6. Estimates of mean annual precipitation (blue) and mean annual temperature (pink) from tooth enamel and bone stable isotope compositions. Shaded areas and colored lines represent the 95% CI of the entire data set. Solid and dashed black lines are the median and 95% CI using data from family Toxodontidae. Green line and shaded area are boron isotope-based atmospheric CO_2 concentrations (Greenop et al., 2014). Shaded gray region corresponds to rapid warming at the onset of the MCO as in Figure 5. (a) MAP calculated using data from all taxa and from only family Toxidontidae shows a decrease from ca. 1,000 mm/yr at the beginning of our record to a minimum of ~500 mm/yr at ~16.9 Ma and a rebound to 800 mm/yr by 16.6 Ma. Toxodontidae data also suggest a high-MAP pulse at 17.0 Ma. Calculated MAP at the beginning of the record is consistent with previous MAP estimates using niche metrics and cenograms (dashed line, MAP > 1,000 mm/yr; Kay, Vizcaino, et al., 2012), fauna and sedimentological evidence (dashed line, MAP < 1,000 mm/yr; Vizcaíno et al., 2010), and tegu lizard fossils (dashed line, MAP > 200 mm/yr; Fernicola & Albino, 2012) are also shown. (b) MAT calculated using all taxa and from only family Toxodontidae shows decreasing MAT to a minimum at ~17.1 Ma (~17°C), a rebound 20–23°C at ~17.0, and an increase to a maximum at the end of the record (26°C). Based on all data, a MAT oscillation occurred at ~16.8 Ma. Calculated MAT at the beginning of the record is consistent with independent constraints based on fossil wood physiognomy (vertical bars; Brea et al., 2012), and tegu lizard fossils (MAP > 14°C; Fernicola & Albino, 2012) are also shown.

We interpret low $\delta^{18}O$ values for *Astrapotherium* as supporting other lines of evidence for a semiaquatic lifestyle.

5.3. Carbon Isotopes and Climate

Two factors complicate our ability to link changes in tooth enamel isotopes to changes in global climate. First, marine proxy records for this time period (Holbourn et al., 2015) have a much higher temporal resolution than our data, and second, our data have considerably higher variance than marine records. We therefore focus on comparisons between marine records and our smoothed and interpolated isotope compositions, rather than raw enamel and bone data. Note that changes in atmospheric CO_2 $\delta^{13}C$ values are reflected as changes to plant carbon isotope compositions in a 1:1 relationship. That is, at constant MAP, an increase in atmospheric CO_2 $\delta^{13}C$ causes an equivalent increase in tooth enamel $\delta^{13}C$. Consequently, it is more important to focus on changes in $\Delta^{13}C$, which reflect MAP, than any specific shift in $\delta^{13}C$.

Overall, our calculations show a trend of decreasing MAP between ~17.4 and ~16.9 Ma (Figure 6), a MAP minimum corresponding to the onset of the MCO at ~16.9 Ma, followed by a rebound to higher MAP by 16.5 Ma. For the 17.4 to 16.9 Ma interval, enamel $\delta^{13}C$ values increased by ~1‰ beginning at ~17.4 Ma to reach a maximum at ~16.9 Ma. Simultaneously, atmospheric CO_2 $\delta^{13}C$ increased only slightly by +0.2‰. In combination, $\Delta^{13}C$ decreased by 0.8‰, indicating a decrease in MAP, specifically from 1,000 ± 235 mm/yr at ~17.4 Ma to 525 ± 105 mm/yr (mean ± 2σ) at ~16.9 Ma (Figure 6).

The onset of the MCO at ~16.9 Ma aligns approximately with the beginning of the "Monterey" carbon isotope excursion toward higher $\delta^{13}C$ values in marine sediments and (inferred) atmospheric CO_2 (Vincent & Berger, 1985). The excursion is thought to have been driven by increased marine and terrestrial productivity and carbon sequestration (Föllmi et al., 2005; Vincent & Berger, 1985), modulated by a series of 400 ka oscillations, which correspond to long period eccentricity (Holbourn et al., 2007; Ma et al., 2011). As interpreted from marine data, the first of these oscillations corresponds to an abrupt warming period between 16.9 and 16.7 Ma, possibly driven by enhanced insolation during high eccentricity (Holbourn et al., 2015). This warming period corresponds to a $\delta^{13}C$ maximum in our smoothed data.

Between 16.9 and 16.7 Ma, atmospheric CO_2 $\delta^{13}C$ values increased by 0.1 to 0.2‰, while median $\delta^{13}C$ values of tooth enamel remained static or decreased slightly (~0.1‰). These trends combine to form an increase in $\Delta^{13}C$ between plants and atmospheric CO_2 and, consequently, an increase in MAP to 685 ± 170 mm/yr.

Between 16.7 and 16.4 Ma, atmospheric CO_2 $\delta^{13}C$ increased by ~0.3‰, while $\delta^{13}C$ of tooth enamel remained approximately constant. The increase in median $\Delta^{13}C$ implies an increase in MAP to 835 ± 270 mm/yr at the end of the record. Within 2σ uncertainty, this estimate overlaps the MAP estimate at ~17.4 Ma (1,000 ± 235 mm/yr) but not the MAP estimate at ~16.9 Ma (525 ± 105 mm/yr).

5.4. Oxygen Isotopes and Climate

Mean enamel and bone $\delta^{18}O$ values varied only slightly from 17.4 to 17.1 Ma. Modeled MAT values during this period are warm (20 ± 4°C; Figure 6), with the exception of a negative excursion at 17.3 Ma. Benthic foraminifera $\delta^{18}O$ values were also stable during this period (17.1–17.4 Ma), pointing to little change to

temperature and/or ice volume (Holbourn et al., 2015). Increasing enamel $\delta^{18}O$ values by ~1‰ and a corresponding decrease in bone $\delta^{18}O$ values at ~17.0 Ma suggest a brief MAT excursion up to 25 ± 7°C at the onset of the MCO. Global warming beginning at about ~16.9 Ma (Holbourn et al., 2015), drove a reduction and reconfiguration of the East Antarctic ice sheet, resulting in an ~0.5‰ decrease in marine $\delta^{18}O$ values as melting ice added ^{18}O depleted water to the oceans (Pekar & Christie-Blick, 2008; Pekar & DeConto, 2006). The retreat of the East Antarctic Ice Sheet inland (Hauptvogel & Passchier, 2012; Passchier et al., 2011; Sangiorgi et al., 2018), coupled with an influx of fresh meltwater into the southern Atlantic, reduced the production of Antarctic bottom water (Pekar & DeConto, 2006). Reduced bottom water production, in turn, weakened thermohaline circulation, inhibiting the transport of warm equatorial waters south during this period (Pekar & DeConto, 2006; Schmitz, 1995). Despite a global temperature increase, the calculated MAT in our section decreased slightly between 17 and 16.7 Ma, with a minimum estimate of 19 ± 4°C, at ~16.85 Ma. This temperature decrease suggests regional cooling, perhaps the result of reduced equatorial heat transport or influx of cold Antarctic water or both. Low observed MAP during this period also suggests that weakened circulation led to lower evaporation and, likely, evapotranspiration.

After ~16.7 Ma, enamel $\delta^{18}O$ values increased slightly, while bone $\delta^{18}O$ values remain constant. Calculated MAT rebounded to high values until the end of the record with a maximum modeled temperature of 25 ± 8°C at 16.5 Ma. This rebound could reflect a temporary stabilization of the reduced Antarctic ice sheet, perhaps permitting warmer low latitude waters to influence Patagonian climate more strongly. Thus, despite an initial excursion toward lower temperatures and precipitation, southern Patagonia ultimately followed global trends in increased temperature and precipitation observed in Northern and Southern Hemispheres records (Böhme, 2003; Böhme et al., 2011; Feakins et al., 2012; Hinojosa & Villagrán, 2005; Reichgelt et al., 2015; Warny et al., 2009; Wolfe, 1985, 1994).

Uplift of the Andes during the Miocene enhanced orographic rain shadow for much of Patagonia, driving a long-term aridification of the area (Blisniuk et al., 2005; Palazzesi et al., 2014). While the magnitude of uplift between 17.4 and 16.5 Ma is unclear, oxygen isotope lapse rates for the southern Andes predict a −0.3‰/0.1 km decrease in $\delta^{18}O$ values with increasing elevation (Blisniuk & Stern, 2005; Poage & Chamberlain, 2001). Given that enamel and bone $\delta^{18}O$ values show a gradual increase, we assume that Andean uplift did not significantly influence meteoric water isotope compositions during this period and that observed changes are a result of larger-scale climatic forcing.

5.5. Isotopic Zoning and Seasonality

Overall, carbon and oxygen isotope zoning within individual teeth is less than 2‰, suggesting small to moderate seasonal change in precipitation and vegetation compositions. Modern precipitation and lake water $\delta^{18}O$ values for the study area each vary by nearly 20‰ (Mayr et al., 2007). Assuming that typical enamel mineralization rates and body water residence times would attenuate the tooth enamel isotopic record of meteoric water variations by ~50% (Kohn, 2004; Passey & Cerling, 2002; Podlesak et al., 2008), modern teeth from the area would be expected to preserve $\delta^{18}O$ variations of ~10‰, much higher than the observed variation in fossil teeth. There must therefore have been little seasonality to precipitation $\delta^{18}O$, likely pointing to less seasonal variation in temperature, congruent with interpretations of climate proxies based on mammalian functional morphology (Kay, Vizcaino, et al., 2012).

5.6. Comparisons to Other Proxies

Most previous MAP and MAT estimates for the Santa Cruz Formation have focused on floras and faunas from several productive faunal levels (Kay, Vizcaino, et al., 2012; Tauber, 1997b) of similar age (~17.4 to ~17.5 Ma; Perkins et al., 2012). Consequently, these estimates represent a short period of time that best corresponds to our oldest strata.

Wood physiognomy-based estimates of MAT (19.3 ± 1.7°C; Brea et al., 2012; Wiemann et al., 1999) from the lower Santa Cruz Formation fall entirely within the uncertainty of our MAT calculations for older fossils (20 ± 4 > 17.2 Ma). An alternative MAT estimate from the same source of 9.4 ± 1.7°C (Brea et al., 2012; Poole et al., 2005) does not overlap our data and is also inconsistent with faunal data suggesting MAT > 14°C (Fernicola & Albino, 2012; Kay, Vizcaino, et al., 2012). As noted by Brea et al. (2012), the lower MAT estimates were based on less than 10 different types of wood, while 20–25 samples are recommended (Wiemann et al., 1999); thus, the temperature discrepancy may reflect sampling bias.

Previously reported estimates of MAP for the Santa Cruz Formation vary significantly, with some estimates mutually exclusive. Published values include <1,000 mm/yr (Vizcaíno et al., 2010), 1,000–1,500 mm/yr (Kay, Vizcaino, et al., 2012), and 850–1,350 mm/yr (Spradley et al., 2019). Wood physiognomy-based MAP calculations are imprecise (870 ± 940 mm/yr; Brea et al., 2012).

Our MAP estimate at ~17.4 Ma (~1,000 ± 235 mm/yr) broadly agrees with these prior estimates.

5.7. Comparisons to General Circulation Models

Most general circulation models of the MCO do not model temporal changes to precipitation and temperature conditions and often focus on broad time slices that may or may not overlap a chronostratigraphic section of interest. In particular, suitable mid-Miocene proxy sites are heterogeneously distributed in both space and time, which requires models to be compared to records that are not necessarily coeval. Recent records from Antarctica (Feakins et al., 2012; Hauptvogel & Passchier, 2012; Passchier et al., 2011; Sangiorgi et al., 2018; Warny et al., 2009) and New Zealand (Reichgelt et al., 2015) improve the number of Southern Hemisphere proxy records, but most terrestrial proxy records still come from Europe and North America (Goldner et al., 2014; Herold et al., 2010). Given these limitations, how accurately do existing models of the MCO predict the physical conditions of the Santa Cruz Formation? For these comparisons, we focus on our youngest results (post 16.6 Ma), that is, after the onset of the MCO.

Our results indicate slightly lower MAP (835 ± 260 mm/yr) than most general circulation models. Herold et al. (2011) and Tong et al. (2009) predict MAP of 1,000–1,200 mm/yr, whereas Henrot et al. (2010) predict MAP lower than our median results (~500 mm/yr). The model of Henrot et al. (2010) also predicts strongly seasonal precipitation, with ~75% occurring in the Southern Hemisphere summer (December-January-February). Conversely, seasonality estimates based on plant macrofossils (Brea et al., 2012) suggest long (7-month) dry summers. Both of these estimates are inconsistent with our enamel zoning profiles, which suggest little seasonal variability.

Our analyses also indicate a significant increase in MAT relative to today (11 ± 4 to 17 ± 7°C), which overlaps estimated increases in summertime temperatures in coastal Antarctica (11 ± 3°C, Feakins et al., 2012). Because the time periods for these two data sets are so different (20–15.5 Ma for Antarctic data; 17.4 to 16.4 for our data), we are reluctant to interpret potential changes in meridional temperature gradients. Model-derived MAT estimates for our study area are consistently too low, when compared to our MAP estimates for post 16.6 Ma, with all models predicting temperatures of ~10°C to 15°C for the study area (Henrot et al., 2010; Herold et al., 2011; Tong et al., 2009). Henrot et al. (2010) and Goldner et al. (2014) noted that their models underestimated MCO warming for high latitudes, primarily by overestimating the meridional temperature gradient, and concluded that more proxy records are needed at these latitudes to constrain physical conditions in these areas. Overall, general circulation models provide accurate estimates of climate parameters at low and middle latitudes but deviate from inferred conditions at high latitudes. Our data provide an additional high latitude record, but more records are likely required for accurate modeling.

6. Conclusions

Our study of carbon and oxygen isotopes from herbivore tooth enamel reveals that global warming at the onset of the MCO (Holbourn et al., 2015) had significant impacts on the climate of Patagonia. MAP initially decreased significantly between 17.4 and 16.9 Ma before stabilizing during the MCO. Regional MAT and MAP reductions at the onset of the MCO suggest that increasing global temperatures and reduced Antarctic ice volume temporarily lowered MAP and MAT in Patagonia. This transitional period in Patagonia was followed by a rebound by ~16.4 Ma to higher MAP and MAT as regional climates began to parallel global increases in temperature and precipitation during the MCO.

Carbon isotope-based MAP and MAT calculations are consistent with most previous floral and faunal estimates, although our ~1 myr record reveals significant fluctuations in both MAP and MAT through time. MAT calculations based on enamel and bone oxygen isotopes also agree with floral and faunal data, revealing temperatures significantly warmer (MAT = 20–25°C) than modern conditions (MAT ~8°C).

Finally, general circulation models consistently underestimate MAT for Miocene Patagonia, perhaps in part because until recently, most MCO proxy records for validation were restricted to the Northern Hemisphere. Our new temperature and precipitation proxy record from the southernmost terrestrial mid-Miocene site in

extreme southern South America may help improve the accuracy of mid-Miocene models. As most models of future atmospheric CO_2 concentrations are similar to or exceed estimates for the MCO (IPCC, 2014), understanding physical conditions and ecology during this time may help provide insight into future climate scenarios for southern South America.

Data Availability Statement

All stable isotope data are available in the supporting information and are hosted in the OSFHome repository at www.osf.io/f28az/.

Acknowledgments

We thank Dr. Samantha Evans for her assistance with stable isotope analyses and three anonymous reviewers for their incisive and comprehensive comments that significantly improved this manuscript. We also thank Dr. Christopher Hill and Dr. Mark Schmitz for their insightful comments on earlier versions of this manuscript. This work was funded by National Science Foundation Grants EAR-1349749 (M. J. K.), EAR-1349741 (R. F. K.), and EAR-1349530 (C. A. E. S.) and also grants UNLP N867, PICT 2013-0389 (S. F. V.), and PICT 2017-1081 (M. S. B.).

References

Avilla, L., & Vizcaíno, S. (2005). *Locomotory pattern of Astrapotherium magnum (Owen) (Mammalia: Astrapotheria) from the Neomiocene (Colhuehuapian–Santacrucian) of Argentina*. Paper Presented at the II Congresso Latino-Americano de Paleontologia de Vertebrados, Rio de Janeiro, Brazil.

Ayliffe, L. K., & Chivas, A. R. (1990). Oxygen isotope composition of the bone phosphate of Australian kangaroos: Potential as a palaeoenvironmental recorder. *Geochimica et Cosmochimica Acta*, *54*(9), 2603–2609. https://doi.org/10.1016/0016-7037(90)90246-H

Ayliffe, L. K., Chivas, A. R., & Leakey, M. G. (1994). The retention of primary oxygen isotope compositions of fossil elephant skeletal phosphate. *Geochimica et Cosmochimica Acta*, *58*(23), 5291–5298. https://doi.org/10.1016/0016-7037(94)90312-3

Balasse, M. (2003). Potential biases in sampling design and interpretation of intra-tooth isotope analysis. *International Journal of Osteoarchaeology*, *13*(1–2), 3–10. https://doi.org/10.1002/oa.656

Balasse, M., Obein, G., Ughetto-Monfrin, J., & Mainland, I. (2012). Investigating seasonality and season of birth in past herds: A reference set of sheep enamel stable oxygen isotope ratios. *Archaeometry*, *54*(2), 349–368. https://doi.org/10.1111/j.1475-4754.2011.00624.x

Bargo, M. S., Toledo, N., & Vizcaino, S. F. (2012). Paleobiology of Santacrucian sloths and anteaters. In S. F. Vizcaíno, R. F. Kay, & M. S. Bargo (Eds.), *Early Miocene paleobiology in Patagonia: High-latitude paleocommunities of the Santa Cruz Formation* (pp. 216–242). New York, NY: Cambridge University Press.

Barreda, V., & Palazzesi, L. (2007). Patagonian vegetation turnovers during the Paleogene-early Neogene: Origin of arid-adapted floras. *The Botanical Review*, *73*(1), 31–50. https://doi.org/10.1663/0006-8101(2007)73[31:PVTDTP]2.0.CO;2

Beerling, D. J., & Royer, D. L. (2011). Convergent Cenozoic CO_2 history. *Nature Geoscience*, *4*(7), 418–420. https://doi.org/10.1038/ngeo1186

Bershaw, J., Garzione, C. N., Higgins, P., MacFadden, B. J., Anaya, F., & Alvarenga, H. (2010). Spatial-temporal changes in Andean plateau climate and elevation from stable isotopes of mammal teeth. *Earth and Planetary Science Letters*, *289*(3–4), 530–538. https://doi.org/10.1016/j.epsl.2009.11.047

Blisniuk, P. M., & Stern, L. A. (2005). Stable isotope paleoaltimetry: A critical review. *American Journal of Science*, *305*(10), 1033–1074. https://doi.org/10.2475/ajs.305.10.1033

Blisniuk, P. M., Stern, L. A., Chamberlain, C. P., Idleman, B., & Zeitler, P. K. (2005). Climatic and ecologic changes during Miocene surface uplift in the southern Patagonian Andes. *Earth and Planetary Science Letters*, *230*(1-2), 125–142. https://doi.org/10.1016/j.epsl.2004.11.015

Böhme, M. (2003). The Miocene Climatic Optimum: Evidence from ectothermic vertebrates of Central Europe. *Palaeogeography, Palaeoclimatology, Palaeoecology*, *195*(3–4), 389–401. https://doi.org/10.1016/S0031-0182(03)00367-5

Böhme, M., Winklhofer, M., & Ilg, A. (2011). Miocene precipitation in Europe: Temporal trends and spatial gradients. *Palaeogeography, Palaeoclimatology, Palaeoecology*, *304*(3-4), 212–218. https://doi.org/10.1016/j.palaeo.2010.09.028

Bown, T. M., & Fleagle, J. G. (1993). Systematics, biostratigraphy, and dental evolution of the Palaeothentidae, later Oligocene to early-middle Miocene (Deseadan-Santacrucian) caenolestoid marsupials of South America. *Memoir (The Paleontological Society)*, 1–76.

Brea, M., Zucol, A., & Iglesias, A. (2012). Fossil plant studies from late Early Miocene of the Santa Cruz Formation: Paleoecology and paleoclimatology at the passive margin of Patagonia, Argentina. In S. F. Vizcaino, R. F. Kay, & M. S. Bargo (Eds.), *Early Miocene paleobiology in Patagonia: High-latitude paleocommunities of the Santa Cruz Formation* (pp. 104–128). Cambridge: Cambridge University Press. https://doi.org/10.1017/CBO9780511667381.008

Brea, M., Zucol, A. F., Bargo, M. S., Fernicola, J. C., & Vizcaíno, S. F. (2017). First Miocene record of Akaniaceae in Patagonia (Argentina): A fossil wood from the early Miocene Santa Cruz Formation and its palaeobiogeographical implications. *Botanical Journal of the Linnean Society*, *183*(3), 334–347. https://doi.org/10.1093/botlinnean/bow014

Buckley, M. (2015). Ancient collagen reveals evolutionary history of the endemic South American 'ungulates'. *Proceedings of the Royal Society B*, *282*(1806), 20142671.

Butzin, M., Lohmann, G., & Bickert, T. (2011). Miocene ocean circulation inferred from marine carbon cycle modeling combined with benthic isotope records. *Paleoceanography*, *26*, PA1203. https://doi.org/10.1029/2009PA001901

Cassini, G., Cerdeño, E., Villafañe, A., & Muñoz, N. (2012). Paleobiology of Santacrucian native ungulates (Meridiungulata: Astrapotheria, Litopterna and Notoungulata). In S. F. Vizcaino, R. F. Kay, & M. S. Bargo (Eds.), *Early Miocene paleobiology in Patagonia: High-latitude paleocommunities of the Santa Cruz Formation* (pp. 243–286). Cambridge, UK: Cambridge University Press. https://doi.org/10.1017/CBO9780511667381.015

Cassini, G. H. (2013). Skull geometric morphometrics and paleoecology of Santacrucian (late early Miocene; Patagonia) native ungulates (Astrapotheria, Litopterna, and Notoungulata). *Ameghiniana*, *50*(2), 193–216. https://doi.org/10.5710/AMGH.7.04.2013.606

Cassini, G. H., & Vizcaíno, S. F. (2012). An approach to the biomechanics of the masticatory apparatus of Early Miocene (Santacrucian Age) South American ungulates (Astrapotheria, Litopterna, and Notoungulata): Moment arm estimation based on 3D landmarks. *Journal of Mammalian Evolution*, *19*(1), 9–25. https://doi.org/10.1007/s10914-011-9179-5

Catena, A. M., & Croft, D. A. (2020). What are the best modern analogs for ancient South American mammal communities? Evidence from ecological diversity analysis (EDA). *Palaeontologia Electronica*, *23*(1).

Cerling, T. E., Harris, J. M., MacFadden, B. J., Leakey, M. G., Quade, J., Eisenmann, V., & Ehleringer, J. R. (1997). Global vegetation change through the Miocene/Pliocene boundary. *Nature*, *389*(6647), 153–158. https://doi.org/10.1038/38229

Clementz, M. T., Holroyd, P. A., & Koch, P. L. (2008). Identifying aquatic habits of herbivorous mammals through stable isotope analysis. *PALAIOS*, *23*(9), 574–585. https://doi.org/10.2110/palo.2007.p07-054r

Cramer, B., Miller, K., Barrett, P., & Wright, J. (2011). Late Cretaceous-Neogene trends in deep ocean temperature and continental ice volume: Reconciling records of benthic foraminiferal geochemistry ($\delta^{18}O$ and Mg/Ca) with sea level history. *Journal of Geophysical Research*, *116*, C12023. https://doi.org/10.1029/2011JC007255

Croft, D. A. (2001). Cenozoic environmental change in South America as indicated by mammalian body size distributions (cenograms). *Diversity and Distributions*, *7*(6), 271–287. https://doi.org/10.1046/j.1366-9516.2001.00117.x

Croft, D. A. (2013). What constitutes a fossil mammal community in the early Miocene Santa Cruz Formation? *Journal of Vertebrate Paleontology*, *33*(2), 401–409. https://doi.org/10.1080/02724634.2013.722154

Cuitiño, J. I., Fernicola, J. C., Kohn, M. J., Trayler, R. B., Naipauer, M., Bargo, M. S., et al. (2016). U-Pb geochronology of the Santa Cruz Formation (early Miocene) at the Río Bote and Río Santa Cruz (southernmost Patagonia, Argentina): Implications for the correlation of fossil vertebrate localities. *Journal of South American Earth Sciences*, *70*, 198–210. https://doi.org/10.1016/j.jsames.2016.05.007

Cuitiño, J. I., & Scasso, R. A. (2010). Sedimentología y paleoambientes del Patagoniano y su transición a la Formación Santa Cruz al sur del Lago Argentino, Patagonia Austral. *Revista de la Asociación Geológica Argentina*, *66*(3), 406–417.

Cuitiño, J. I., Ventura Santos, R., Alonso Muruaga, P. J., & Scasso, R. A. (2015). Sr-stratigraphy and sedimentary evolution of early Miocene marine foreland deposits in the northern Austral (Magallanes) Basin, Argentina. *Andean Geology*, *42*(3).

Diefendorf, A. F., Mueller, K. E., Wing, S. L., Koch, P. L., & Freeman, K. H. (2010). Global patterns in leaf ^{13}C discrimination and implications for studies of past and future climate. *Proceedings of the National Academy of Sciences*, *107*(13), 5738–5743. https://doi.org/10.1073/pnas.0910513107

Driessens, F. C., & Verbeeck, R. (1990). *Biominerals*. Boca Raton, FL: CRC Press.

Dunn, R. E., Strömberg, C. A., Madden, R. H., Kohn, M. J., & Carlini, A. A. (2015). Linked canopy, climate, and faunal change in the Cenozoic of Patagonia. *Science*, *347*(6219), 258–261. https://doi.org/10.1126/science.1260947

Edwards, E. J., & Ogburn, R. M. (2012). Angiosperm responses to a low-CO_2 world: CAM and C_4 photosynthesis as parallel evolutionary trajectories. *International Journal of Plant Sciences*, *173*(6), 724–733. https://doi.org/10.1086/666098

Edwards, E. J., Osborne, C. P., Strömberg, C. A., Smith, S. A., & Consortium, C. G. (2010). The origins of C_4 grasslands: Integrating evolutionary and ecosystem science. *Science*, *328*(5978), 587–591.

Ehleringer, J. R. (1989). Carbon isotope ratios and physiological processes in aridland plants. In *Stable isotopes in ecological research* (pp. 41–54). New York: Springer.

Ehleringer, J. R., & Cooper, T. A. (1988). Correlations between carbon isotope ratio and microhabitat in desert plants. *Oecologia*, *76*(4), 562–566. https://doi.org/10.1007/BF00397870

Elissamburu, A. (2010). Estudio biomecánico y morfofuncional del esqueleto apendicular de Homalodotherium Flower 1873 (Mammalia, Notoungulata). *Ameghiniana*, *47*(1), 25–43. https://doi.org/10.5710/AMGH.v47i1.2

Elliott, J. C. (2002). Calcium phosphate biominerals. *Reviews in Mineralogy and Geochemistry*, *48*(1), 427–453. https://doi.org/10.2138/rmg.2002.48.11

Farquhar, G. D., Ehleringer, J. R., & Hubick, K. T. (1989). Carbon isotope discrimination and photosynthesis. *Annual Review of Plant Biology*, *40*(1), 503–537. https://doi.org/10.1146/annurev.pp.40.060189.002443

Feakins, S. J., Warny, S., & Lee, J.-E. (2012). Hydrologic cycling over Antarctica during the middle Miocene warming. *Nature Geoscience*, *5*(8), 557–560. https://doi.org/10.1038/ngeo1498

Feranec, R., & MacFadden, B. (2006). Isotopic discrimination of resource partitioning among ungulates in C_3-dominated communities from the Miocene of Florida and California. *Paleobiology*, *32*(2), 191–205. https://doi.org/10.1666/05006.1

Fernicola, J., & Albino, A. (2012). Amphibians and squamate reptiles from the Santa Cruz Formation (late Early Miocene), Santa Cruz Province, Argentina: Paleoenvironmental and paleobiological considerations. In *Early Miocene paleobiology in patagonia: High-latitude paleocommunities of the Santa Cruz Formation* (pp. 129–137). New York: Cambridge University Press.

Fernicola, J. C., Bargo, M. S., Vizcaíno, S. F., & Kay, R. F. (2019). Early–Middle Miocene paleontology in the Río Santa Cruz, southern Patagonia, Argentina. 130 Years Since Ameghino, 1887. *Publicación Electrónica de la Asociación Paleontológica Argentina*, *19*(2), 1–259.

Fleagle, J. G., Bown, T., Swisher, C., & Buckley, G. (1995). *Age of the Pinturas and Santa Cruz Formations*. Paper presented at the Congreso Argentino de Paleontología y Bioestratigrafía.

Fleagle, J. G., Perkins, M. E., Heizler, M. T., Nash, B., Bown, T. M., Tauber, A. A., et al. (2012). Absolute and relative ages of fossil localities in the Santa Cruz and Pinturas Formations. In S. F. Vizcaíno, R. F. Kay, & M. S. Bargo (Eds.), *Early Miocene paleobiology in Patagonia: High-latitude paleocommunities of the Santa Cruz Formation* (pp. 41–58). New York, NY: Cambridge University Press.

Fletcher, T. M., Janis, C. M., & Rayfield, E. J. (2010). Finite element analysis of ungulate jaws: Can mode of digestive physiology be determined. *Palaeontologia Electronica*, *13*(3).

Flower, B. P., & Kennett, J. P. (1993). Relations between Monterey Formation deposition and middle Miocene global cooling: Naples Beach section, California. *Geology*, *21*(10), 877–880. https://doi.org/10.1130/0091-7613(1993)021<0877:RBMFDA>2.3.CO;2

Flower, B. P., & Kennett, J. P. (1994). The middle Miocene climatic transition: East Antarctic ice sheet development, deep ocean circulation and global carbon cycling. *Palaeogeography, Palaeoclimatology, Palaeoecology*, *108*(3–4), 537–555. https://doi.org/10.1016/0031-0182(94)90251-8

Föllmi, K. B., Badertscher, C., de Kaenel, E., Stille, P., John, C. M., Adatte, T., & Steinmann, P. (2005). Phosphogenesis and organic-carbon preservation in the Miocene Monterey Formation at Naples Beach, California—The Monterey hypothesis revisited. *Geological Society of America Bulletin*, *117*(5), 589–619. https://doi.org/10.1130/B25524.1

Fricke, H. C., Clyde, W. C., & O'Neil, J. R. (1998). Intra-tooth variations in $\delta^{18}O$ (PO_4) of mammalian tooth enamel as a record of seasonal variations in continental climate variables. *Geochimica et Cosmochimica Acta*, *62*(11), 1839–1850. https://doi.org/10.1016/S0016-7037(98)00114-8

Fricke, H. C., & O'Neil, J. R. (1996). Inter-and intra-tooth variation in the oxygen isotope composition of mammalian tooth enamel phosphate: Implications for palaeoclimatological and palaeobiological research. *Palaeogeography, Palaeoclimatology, Palaeoecology*, *126*(1-2), 91–99. https://doi.org/10.1016/S0031-0182(96)00072-7

Gasson, E., DeConto, R. M., Pollard, D., & Levy, R. H. (2016). Dynamic Antarctic ice sheet during the early to mid-Miocene. *Proceedings of the National Academy of Sciences*, *113*(13), 3459–3464. https://doi.org/10.1073/pnas.1516130113

Goldner, A., Herold, N., & Huber, M. (2014). The challenge of simulating the warmth of the mid-Miocene climatic optimum in CESM1. *Climate of the Past*, *10*(2), 523–536. https://doi.org/10.5194/cp-10-523-2014

Green, D. R., Smith, T. M., Green, G. M., Bidlack, F. B., Tafforeau, P., & Colman, A. S. (2018). Quantitative reconstruction of seasonality from stable isotopes in teeth. *Geochimica et Cosmochimica Acta*, *235*, 483–504. https://doi.org/10.1016/j.gca.2018.06.013

Greenop, R., Foster, G. L., Wilson, P. A., & Lear, C. H. (2014). Middle Miocene climate instability associated with high-amplitude CO_2 variability. *Paleoceanography*, *29*, 845–853. https://doi.org/10.1002/2014PA002653

Harris, E. B., Kohn, M. J., & Strömberg, C. A. (2020). Stable isotope compositions of herbivore teeth indicate climatic stability leading into the middle Miocene Climatic Optimum, in Idaho, USA. *Palaeogeography, Palaeoclimatology, Palaeoecology*, 109610.

Hartnady, C., & Le Roex, A. (1985). Southern Ocean hotspot tracks and the Cenozoic absolute motion of the African, Antarctic, and South American plates. *Earth and Planetary Science Letters*, *75*(2–3), 245–257. https://doi.org/10.1016/0012-821X(85)90106-2

Haslett, J., & Parnell, A. C. (2008). A simple monotone process with application to radiocarbon-dated depth chronologies. *Applied Statistics*, *57*(4), 399–418.

Hauptvogel, D. W., & Passchier, S. (2012). Early–Middle Miocene (17–14 Ma) Antarctic ice dynamics reconstructed from the heavy mineral provenance in the AND-2A drill core, Ross Sea, Antarctica. *Global and Planetary Change*, *82*, 38–50.

Henrot, A.-J., François, L., Favre, E., Butzin, M., Ouberdous, M., & Munhoven, G. (2010). Effects of CO_2, continental distribution, topography and vegetation changes on the climate at the Middle Miocene: A model study. *Climate of the Past*, *6*(5), 675–694. https://doi.org/10.5194/cp-6-675-2010

Herold, N., Huber, M., & Müller, R. (2011). Modeling the Miocene Climatic Optimum. Part I: Land and atmosphere. *Journal of Climate*, *24*(24), 6353–6372. https://doi.org/10.1175/2011JCLI4035.1

Herold, N., Müller, R., & Seton, M. (2010). Comparing early to middle Miocene terrestrial climate simulations with geological data. *Geosphere*, *6*(6), 952–961. https://doi.org/10.1130/GES00544.1

Hinojosa, L. F., & Villagrán, C. (2005). Did South American mixed paleofloras evolve under thermal equability or in the absence of an effective Andean barrier during the Cenozoic? *Palaeogeography, Palaeoclimatology, Palaeoecology*, *217*(1–2), 1–23. https://doi.org/10.1016/j.palaeo.2004.11.013

Holbourn, A., Kuhnt, W., Kochhann, K. G., Andersen, N., & Meier, K. S. (2015). Global perturbation of the carbon cycle at the onset of the Miocene Climatic Optimum. *Geology*, *43*(2), 123–126. https://doi.org/10.1130/G36317.1

Holbourn, A., Kuhnt, W., Schulz, M., Flores, J.-A., & Andersen, N. (2007). Orbitally-paced climate evolution during the middle Miocene "Monterey" carbon-isotope excursion. *Earth and Planetary Science Letters*, *261*(3-4), 534–550. https://doi.org/10.1016/j.epsl.2007.07.026

Hoppe, K. (2006). Correlation between the oxygen isotope ratio of North American bison teeth and local waters: Implication for paleoclimatic reconstructions. *Earth and Planetary Science Letters*, *244*(1–2), 408–417. https://doi.org/10.1016/j.epsl.2006.01.062

IPCC (2014). *Climate change 2014: Synthesis report, Contribution of Working Groups I, II and III to the Fifth Assessment Report of the Intergovernmental Panel on Climate Change.* Geneva, Switzerland.

Kay, R. F., Perry, J. M., Malinzak, M., Allen, K. L., Kirk, E. C., Plavcan, J. M., & Fleagle, J. (2012). The paleobiology of Santacrucian primates. In S. F. Vizcaíno, M. R. F. Kay, & M. S. Bargo (Eds.), *Early Miocene paleobiology in Patagonia: High-latitude paleocommunities of the Santa Cruz Formation* (pp. 306–330). New York, NY: Cambridge University Press. https://doi.org/10.1017/CBO9780511667381.017

Kay, R. F., Vizcaino, S. F., & Bargo, M. S. (2012). A review of the paleoenvironment and paleoecology of the Miocene Santa Cruz Formation. In S. F. Vizcaíno, R. F. Kay, & M. S. Bargo (Eds.), *Early Miocene paleobiology in Patagonia: High-latitude paleocommunities of the Santa Cruz Formation* (pp. 331–365). Cambridge: Cambridge University Press. https://doi.org/10.1017/CBO9780511667381.018

Kim, S.-T., & O'Neil, J. R. (1997). Equilibrium and nonequilibrium oxygen isotope effects in synthetic carbonates. *Geochimica et Cosmochimica Acta*, *61*(16), 3461–3475. https://doi.org/10.1016/S0016-7037(97)00169-5

Koch, P., Tuross, N., & Fogel, M. (1997). The effects of sample treatment and diagenesis on the isotopic integrity of carbonate in biogenic hydroxylapatite. *Journal of Archaeological Science*, *24*(5), 417–429. https://doi.org/10.1006/jasc.1996.0126

Kohn, M. (2010). Carbon isotope composition of terrestrial C_3 plants as indicators of (paleo)ecology and (paleo)climate. *Proceedings of the National Academy of Sciences*, *107*, 46.

Kohn, M. (2016). Carbon isotope discrimination in C_3 land plants is independent of natural variations in pCO_2. *Geochemical Perspectives Letters*, *2*, 35–43.

Kohn, M. J. (1996). Predicting animal $\delta^{18}O$: Accounting for diet and physiological adaptation. *Geochimica et Cosmochimica Acta*, *60*(23), 4811–4829. https://doi.org/10.1016/S0016-7037(96)00240-2

Kohn, M. J. (2004). Comment: Tooth enamel mineralization in ungulates: Implications for recovering a primary isotopic time-series, by B. H. Passey and T. E. Cerling (2002). *Geochimica et Cosmochimica Acta*, *68*(2), 403–405.

Kohn, M. J., & Cerling, T. E. (2002). Stable isotope compositions of biological apatite. *Reviews in Mineralogy and Geochemistry*, *48*(1), 455–488. https://doi.org/10.2138/rmg.2002.48.12

Kohn, M. J., & Dettman, D. L. (2007). Paleoaltimetry from stable isotope compositions of fossils. *Reviews in Mineralogy and Geochemistry*, *66*(1), 119–154. https://doi.org/10.2138/rmg.2007.66.5

Kohn, M. J., & Law, J. M. (2006). Stable isotope chemistry of fossil bone as a new paleoclimate indicator. *Geochimica et Cosmochimica Acta*, *70*(4), 931–946. https://doi.org/10.1016/j.gca.2005.10.023

Kohn, M. J., McKay, M. P., & Knight, J. L. (2005). Dining in the Pleistocene—Who's on the menu? *Geology*, *33*(8), 649–652. https://doi.org/10.1130/G21476AR.1

Kohn, M. J., Schoeninger, M. J., & Valley, J. W. (1996). Herbivore tooth oxygen isotope compositions: Effects of diet and physiology. *Geochimica et Cosmochimica Acta*, *60*(20), 3889–3896. https://doi.org/10.1016/0016-7037(96)00248-7

Kohn, M. J., Schoeninger, M. J., & Valley, J. W. (1998). Variability in oxygen isotope compositions of herbivore teeth: Reflections of seasonality or developmental physiology? *Chemical Geology*, *152*(1-2), 97–112. https://doi.org/10.1016/S0009-2541(98)00099-0

Kohn, M. J., Strömberg, C. A. E., Madden, R. H., Dunn, R. E., Evans, S., Palacios, A., & Carlini, A. A. (2015). Quasi-static Eocene-Oligocene climate in Patagonia promotes slow faunal evolution and mid-Cenozoic global cooling. *Palaeogeography, Palaeoclimatology, Palaeoecology*, *435*, 24–37. https://doi.org/10.1016/j.palaeo.2015.05.028

Kürschner, W. M., Kvaček, Z., & Dilcher, D. L. (2008). The impact of Miocene atmospheric carbon dioxide fluctuations on climate and the evolution of terrestrial ecosystems. *Proceedings of the National Academy of Sciences*, *105*(2), 449–453. https://doi.org/10.1073/pnas.0708588105

Laurie, W., Lang, E., & Groves, C. (1983). Rhinoceros unicornis. *Mammalian Species*, *211*, 1–6.

Levin, N. E., Cerling, T. E., Passey, B. H., Harris, J. M., & Ehleringer, J. R. (2006). A stable isotope aridity index for terrestrial environments. *Proceedings of the National Academy of Sciences*, *103*(30), 11201–11205. https://doi.org/10.1073/pnas.0604719103

Luz, B., & Kolodny, Y. (1985). Oxygen isotope variations in phosphate of biogenic apatites, IV. Mammal teeth and bones. *Earth and Planetary Science Letters*, *75*(1), 29–36. https://doi.org/10.1016/0012-821X(85)90047-0

Luz, B., Cormie, A. B., & Schwarcz, H. P. (1990). Oxygen isotope variations in phosphate of deer bones. *Geochimica et Cosmochimica Acta*, *54*(6), 1723–1728. https://doi.org/10.1016/0016-7037(90)90403-8

Ma, W., Tian, J., Li, Q., & Wang, P. (2011). Simulation of long eccentricity (400-kyr) cycle in ocean carbon reservoir during Miocene Climate Optimum: Weathering and nutrient response to orbital change. *Geophysical Research Letters*, *38*, L10701. https://doi.org/10.1029/2011GL047680

MacFadden, B. J. (1998). Tale of two rhinos: Isotopic ecology, paleodiet, and niche differentiation of Aphelops and Teleoceras from the Florida Neogene. *Paleobiology*, *24*(2), 274–286.

Marshall, L. G. (1976). Fossil localities for Santacrucian (early Miocene) mammals, Santa Cruz Province, southern Patagonia, Argentina. *Journal of Paleontology*, 1129–1142.

Matheos, S. D., & Raigemborn, M. S. (2012). Sedimentology and paleoenvironment of the Santa Cruz Formation. In S. F. Vizcaíno, R. F. Kay, & M. S. Bargo (Eds.), *Early Miocene paleobiology in Patagonia: High-latitude paleocommunities of the Santa Cruz Formation* (pp. 59–82). Cambridge: Cambridge University Press. https://doi.org/10.1017/CBO9780511667381.005

Mayr, C., Lücke, A., Stichler, W., Trimborn, P., Ercolano, B., Oliva, G., et al. (2007). Precipitation origin and evaporation of lakes in semi-arid Patagonia (Argentina) inferred from stable isotopes ($\delta^{18}O$, $\delta^{2}H$). *Journal of Hydrology*, *334*(1–2), 53–63. https://doi.org/10.1016/j.jhydrol.2006.09.025

Pagani, M., Arthur, M. A., & Freeman, K. H. (1999). Miocene evolution of atmospheric carbon dioxide. *Paleoceanography*, *14*(3), 273–292. https://doi.org/10.1029/1999PA900006

Pagani, M., Zachos, J. C., Freeman, K. H., Tipple, B., & Bohaty, S. (2005). Marked decline in atmospheric carbon dioxide concentrations during the Paleogene. *Science*, *309*(5734), 600–603. https://doi.org/10.1126/science.1110063

Palazzesi, L., & Barreda, V. (2012). Fossil pollen records reveal a late rise of open-habitat ecosystems in Patagonia. *Nature Communications*, *3*(1), 1294. https://doi.org/10.1038/ncomms2299

Palazzesi, L., Barreda, V. D., Cuitiño, J. I., Guler, M. V., Tellería, M. C., & Santos, R. V. (2014). Fossil pollen records indicate that Patagonian desertification was not solely a consequence of Andean uplift. *Nature Communications*, *5*(1), 3558. https://doi.org/10.1038/ncomms4558

Pascual, R., & Ortiz Jaureguizar, E. (1990). Evolving climates and mammal faunas in Cenozoic South America. In J. Fleagle & A. L. Rosenberger (Eds.), *The Platyrrhine fossil record* (pp. 23–60). San Diego, CA: Academic Press Limited.

Passchier, S., Browne, G., Field, B., Fielding, C., Krissek, L., Panter, K., Pekar, S. F., & ANDRILL-SMS Science Team (2011). Early and middle Miocene Antarctic glacial history from the sedimentary facies distribution in the AND-2A drill hole, Ross Sea, Antarctica. *Bulletin*, *123*(11–12), 2352–2365.

Passey, B. H., & Cerling, T. E. (2002). Tooth enamel mineralization in ungulates: Implications for recovering a primary isotopic time-series. *Geochimica et Cosmochimica Acta*, *66*(18), 3225–3234. https://doi.org/10.1016/S0016-7037(02)00933-X

Passey, B. H., Cerling, T. E., Schuster, G. T., Robinson, T. F., Roeder, B. L., & Krueger, S. K. (2005). Inverse methods for estimating primary input signals from time-averaged isotope profiles. *Geochimica et Cosmochimica Acta*, *69*(16), 4101–4116. https://doi.org/10.1016/j.gca.2004.12.002

Passey, B. H., Robinson, T. F., Ayliffe, L. K., Cerling, T. E., Sponheimer, M., Dearing, M. D., et al. (2005). Carbon isotope fractionation between diet, breath CO_2, and bioapatite in different mammals. *Journal of Archaeological Science*, *32*(10), 1459–1470. https://doi.org/10.1016/j.jas.2005.03.015

Paul, K. I., Polglase, P. J., Smethurst, P. J., O'Connell, A. M., Carlyle, C. J., & Khanna, P. K. (2004). Soil temperature under forests: A simple model for predicting soil temperature under a range of forest types. *Agricultural and Forest Meteorology*, *121*(3–4), 167–182. https://doi.org/10.1016/j.agrformet.2003.08.030

Pekar, S. F., & Christie-Blick, N. (2008). Resolving apparent conflicts between oceanographic and Antarctic climate records and evidence for a decrease in pCO_2 during the Oligocene through early Miocene (34–16 Ma). *Palaeogeography, Palaeoclimatology, Palaeoecology*, *260*(1–2), 41–49. https://doi.org/10.1016/j.palaeo.2007.08.019

Pekar, S. F., & DeConto, R. M. (2006). High-resolution ice-volume estimates for the early Miocene: Evidence for a dynamic ice sheet in Antarctica. *Palaeogeography, Palaeoclimatology, Palaeoecology*, *231*(1-2), 101–109. https://doi.org/10.1016/j.palaeo.2005.07.027

Perkins, M. E., Fleagle, J. G., Heizler, M. T., Nash, B., Bown, T., Tauber, A., & Dozo, M. (2012). Tephrochronology of the Miocene Santa Cruz and Pinturas Formations, Argentina. In S. F. Vizcaíno, R. F. Kay, & M. S. Bargo (Eds.), *Early Miocene paleobiology in Patagonia: High-latitude paleocommunities of the Santa Cruz Formation* (pp. 23–40). New York, NY: Cambridge University Press.

Poage, M. A., & Chamberlain, C. P. (2001). Empirical relationships between elevation and the stable isotope composition of precipitation and surface waters: Considerations for studies of paleoelevation change. *American Journal of Science*, *301*(1), 1–15. https://doi.org/10.2475/ajs.301.1.1

Podlesak, D. W., Torregrossa, A.-M., Ehleringer, J. R., Dearing, M. D., Passey, B. H., & Cerling, T. E. (2008). Turnover of oxygen and hydrogen isotopes in the body water, CO_2, hair, and enamel of a small mammal. *Geochimica et Cosmochimica Acta*, *72*(1), 19–35. https://doi.org/10.1016/j.gca.2007.10.003

Poole, I., Cantrill, D., & Utescher, T. (2005). A multi-proxy approach to determine Antarctic terrestrial palaeoclimate during the Late Cretaceous and Early Tertiary. *Palaeogeography, Palaeoclimatology, Palaeoecology*, *222*(1–2), 95–121. https://doi.org/10.1016/j.palaeo.2005.03.011

R Core Team. (2019). *R: A language and environment for statistical computing*. Vienna, Austria: R Foundation for Statistical Computing. Retrieved from https://www.R-project.org

Raigemborn, M. S., Krapovickas, V., Beilinson, E., Peral, L. E. G., Zucol, A. F., Zapata, L., et al. (2018). Multiproxy studies of Early Miocene pedogenic calcretes in the Santa Cruz Formation of southern Patagonia, Argentina indicate the existence of a temperate warm vegetation adapted to a fluctuating water table. *Palaeogeography, Palaeoclimatology, Palaeoecology*, *500*, 1–23. https://doi.org/10.1016/j.palaeo.2018.03.037

Raigemborn, M. S., Matheos, S. D., Krapovickas, V., Vizcaíno, S. F., Bargo, M. S., Kay, R. F., et al. (2015). Paleoenvironmental reconstruction of the coastal Monte Léon and Santa Cruz formations (Early Miocene) at Rincón del Buque, southern Patagonia: A revisited locality. *Journal of South American Earth Sciences*, *60*, 31–55. https://doi.org/10.1016/j.jsames.2015.03.001

Reichgelt, T., Kennedy, E. M., Conran, J. G., Mildenhall, D. C., & Lee, D. E. (2015). The early Miocene paleolake Manuherikia: Vegetation heterogeneity and warm-temperate to subtropical climate in southern New Zealand. *Journal of Paleolimnology*, *53*(4), 349–365. https://doi.org/10.1007/s10933-015-9827-5

Retallack, G. J. (2009). Refining a pedogenic-carbonate CO_2 paleobarometer to quantify a middle Miocene greenhouse spike. *Palaeogeography, Palaeoclimatology, Palaeoecology*, *281*(1-2), 57–65. https://doi.org/10.1016/j.palaeo.2009.07.011

Robinson, C., Briggs, H., Atkinson, P., & Weatherell, J. (1979). Matrix and mineral changes in developing enamel. *Journal of Dental Research*, *58*(2_suppl), 871–882. https://doi.org/10.1177/00220345790580024101

Robinson, C., Fuchs, P., Deutsch, D., & Weatherell, J. (1978). Four chemically distinct stages in developing enamel from bovine incisor teeth. *Caries Research*, *12*(1), 1–11. https://doi.org/10.1159/000260309

Sage, R. F., Christin, P.-A., & Edwards, E. J. (2011). The C_4 plant lineages of planet Earth. *Journal of Experimental Botany*, *62*(9), 3155–3169. https://doi.org/10.1093/jxb/err048

Sangiorgi, F., Bijl, P. K., Passchier, S., Salzmann, U., Schouten, S., McKay, R., et al. (2018). Southern Ocean warming and Wilkes Land ice sheet retreat during the mid-Miocene. *Nature Communications*, *9*(1), 317. https://doi.org/10.1038/s41467-017-02609-7

Schmitz, W. J. (1995). On the interbasin-scale thermohaline circulation. *Reviews of Geophysics*, *33*(2), 151–173. https://doi.org/10.1029/95RG00879

Schubert, B. A., & Jahren, A. H. (2012). The effect of atmospheric CO_2 concentration on carbon isotope fractionation in C_3 land plants. *Geochimica et Cosmochimica Acta*, *96*, 29–43. https://doi.org/10.1016/j.gca.2012.08.003

Shevenell, A. E., Kennett, J. P., & Lea, D. W. (2004). Middle Miocene southern ocean cooling and Antarctic cryosphere expansion. *Science*, *305*(5691), 1766–1770. https://doi.org/10.1126/science.1100061

Spradley, J. P., Glazer, B. J., & Kay, R. F. (2019). Mammalian faunas, ecological indices, and machine-learning regression for the purpose of paleoenvironment reconstruction in the Miocene of South America. *Palaeogeography, Palaeoclimatology, Palaeoecology*, *518*, 155–171. https://doi.org/10.1016/j.palaeo.2019.01.014

Still, C. J., Berry, J. A., Collatz, G. J., & DeFries, R. S. (2003). Global distribution of C_3 and C_4 vegetation: Carbon cycle implications. *Global Biogeochemical Cycles*, *17*(1), 1006. https://doi.org/10.1029/2001GB001807

Strömberg, C. A., Dunn, R. E., Madden, R. H., Kohn, M. J., & Carlini, A. A. (2013). Decoupling the spread of grasslands from the evolution of grazer-type herbivores in South America. *Nature Communications*, *4*(1), 1478. https://doi.org/10.1038/ncomms2508

Suga, S. (1982). Progressive mineralization pattern of developing enamel during the maturation stage. *Journal of Dental Research*, *61*, 1532–1542.

Tauber, A. A. (1994). *Estratigrafia y vertebrados fósiles de la Formación Santa Cruz (Mioceno inferior) en la costa atlántica entre las rías del Coyle y Río Gallegos, Provincia de Santa Cruz, República Argentina* (Unpublished Dissertation). Argentina: Universidad Nacional de Córdoba.

Tauber, A. A. (1997a). Bioestratigrafía de la Formación Santa Cruz (Mioceno Inferior) en el extremo sudeste de la Patagonia. *Ameghiniana*, *34*(4), 413–426.

Tauber, A. A. (1997b). Paleoecología de la Formación Santa Cruz (Mioceno inferior) en el extremo sudeste de la Patagonia. *Ameghiniana*, *34*(4), 517–529.

Tipple, B. J., Meyers, S. R., & Pagani, M. (2010). Carbon isotope ratio of Cenozoic CO_2: A comparative evaluation of available geochemical proxies. *Paleoceanography*, *25*, PA3202. https://doi.org/10.1029/2009PA001851

Tong, J., You, Y., Müller, R., & Seton, M. (2009). Climate model sensitivity to atmospheric CO_2 concentrations for the middle Miocene. *Global and Planetary Change*, *67*(3–4), 129–140. https://doi.org/10.1016/j.gloplacha.2009.02.001

Townsend, K. B., & Croft, D. A. (2008). Diets of notoungulates from the Santa Cruz Formation, Argentina: New evidence from enamel microwear. *Journal of Vertebrate Paleontology*, *28*(1), 217–230.

Trayler, R. B., Dundas, R. G., Fox-Dobbs, K., & Van de Water, P. K. (2015). Inland California during the Pleistocene-Megafaunal stable isotope records reveal new paleoecological and paleoenvironmental insights. *Palaeogeography Palaeoclimatology Palaeoecology*, *437*, 132–140.

Trayler, R. B., & Kohn, M. J. (2017). Tooth enamel maturation reequilibrates oxygen isotope compositions and supports simple sampling methods. *Geochimica et Cosmochimica Acta*, *198*, 32–47. <Go to ISI>://WOS:000390987900003

Trayler, R. B., Schmitz, M. D., Cuitiño, J. I., Kohn, M. J., Bargo, M. S., Kay, R. F., et al. (2020). An improved approach to age-depth modeling in deep time: Implications for the Santa Cruz Formation, Argentina. *Geological Society of America Bulletin*, *132*(1–2), 233–244. https://doi.org/10.1130/B35203.1

Trueman, C. N., & Tuross, N. (2002). Trace elements in recent and fossil bone apatite. *Reviews in Mineralogy and Geochemistry*, *48*(1), 489–521. https://doi.org/10.2138/rmg.2002.48.13

van der Merwe, N. J., & Medina, E. (1991). The canopy effect, carbon isotope ratios and foodwebs in Amazonia. *Journal of Archaeological Science*, *18*(3), 249–259. https://doi.org/10.1016/0305-4403(91)90064-V

Vincent, E., & Berger, W. H. (1985). Carbon dioxide and polar cooling in the Miocene: The Monterey hypothesis. In E. T. Sundquist & W. S. Broecker (Eds.), *The carbon cycle and atmospheric CO: Natural variations Archean to present* (pp. 455–468). Washington, DC: American Geophysical Union.

Vizcaíno, S. F., Bargo, M. S., Kay, R. F., Fariña, R. A., Di Giacomo, M., Perry, J. M., et al. (2010). A baseline paleoecological study for the Santa Cruz Formation (Late–Early Miocene) at the Atlantic Coast of Patagonia, Argentina. *Palaeogeography, Palaeoclimatology, Palaeoecology*, *292*(3-4), 507–519. https://doi.org/10.1016/j.palaeo.2010.04.022

Vizcaíno, S. F., Bargo, M. S., Kay, R. F., & Milne, N. (2006). The armadillos (Mammalia, Xenarthra, Dasypodidae) of the Santa Cruz Formation (Early–Middle Miocene): An approach to their paleobiology. *Palaeogeography, Palaeoclimatology, Palaeoecology*, *237*(2–4), 255–269. https://doi.org/10.1016/j.palaeo.2005.12.006

Vizcaíno, S. F., Kay, R. F., & Bargo, M. S. (2012a). Background for a paleoecological study of the Santa Cruz Formation (Late Early Miocene) on the Atlantic Coast of Patagonia. In S. F. Vizcaíno, R. F. Kay, & M. S. Bargo (Eds.), *Early Miocene paleobiology in Patagonia: High-latitude paleocommunities of the Santa Cruz Formation* (pp. 1–22). New York, NY: Cambridge University Press.

Vizcaíno, S. F., Kay, R. F., & Bargo, M. S. (2012b). *Early Miocene paleobiology in Patagonia: High-latitude paleocommunities of the Santa Cruz Formation*. Cambridge: Cambridge University Press. https://doi.org/10.1017/CBO9780511667381

Warny, S., Askin, R. A., Hannah, M. J., Mohr, B. A., Raine, J. I., Harwood, D. M., Florindo, F., & the SMS Science Team (2009). Palynomorphs from a sediment core reveal a sudden remarkably warm Antarctica during the middle Miocene. *Geology*, *37*(10), 955–958. https://doi.org/10.1130/G30139A.1

Welker, F., Collins, M. J., Thomas, J. A., Wadsley, M., Brace, S., Cappellini, E., et al. (2015). Ancient proteins resolve the evolutionary history of Darwin's South American ungulates. *Nature*, *522*(7554), 81–84. https://doi.org/10.1038/nature14249

West, E. (1952). A study of the annual soil temperature wave. *Australian Journal of Chemistry*, *5*(2), 303–314. https://doi.org/10.1071/CH9520303

Wiemann, M. C., Manchester, S. R., & Wheeler, E. A. (1999). Paleotemperature estimation from dicotyledonous wood anatomical characters. *PALAIOS*, *14*(5), 459–474. https://doi.org/10.2307/3515397

Wolfe, J. A. (1985). Distribution of major vegetational types during the tertiary. In E. T. Sundquist & W. S. Broecker (Eds.), *The carbon cycle and atmospheric CO: Natural variations Archean to present* (pp. 357–375). Washington, DC: American Geophysical Union.

Wolfe, J. A. (1994). Tertiary climatic changes at middle latitudes of western North America. *Palaeogeography, Palaeoclimatology, Palaeoecology*, *108*(3-4), 195–205. https://doi.org/10.1016/0031-0182(94)90233-X

You, Y., Huber, M., Müller, R., Poulsen, C., & Ribbe, J. (2009). Simulation of the Middle Miocene climate optimum. *Geophysical Research Letters*, *36*, L04702. https://doi.org/10.1029/2008GL036571

Zachos, J., Pagani, M., Sloan, L., Thomas, E., & Billups, K. (2001). Trends, rhythms, and aberrations in global climate 65 Ma to present. *Science*, *292*(5517), 686–693. https://doi.org/10.1126/science.1059412

Zanazzi, A., Kohn, M. J., MacFadden, B. J., & Terry, D. O. (2007). Large temperature drop across the Eocene–Oligocene transition in Central North America. *Nature*, *445*(7128), 639–642. https://doi.org/10.1038/nature05551

Zazzo, A., Balasse, M., & Patterson, W. P. (2005). High-resolution $\delta^{13}C$ intratooth profiles in bovine enamel: Implications for mineralization pattern and isotopic attenuation. *Geochimica et Cosmochimica Acta*, *69*(14), 3631–3642. https://doi.org/10.1016/j.gca.2005.02.031

Zazzo, A., Lécuyer, C., & Mariotti, A. (2004). Experimentally-controlled carbon and oxygen isotope exchange between bioapatites and water under inorganic and microbially-mediated conditions. *Geochimica et Cosmochimica Acta*, *68*(1), 1–12. https://doi.org/10.1016/S0016-7037(03)00278-3

Zazzo, A., Lécuyer, C., Sheppard, S. M. F., Grandjean, P., & Mariotti, A. (2004). Diagenesis and the reconstruction of paleoenvironments: A method to restore original $\delta^{18}O$ values of carbonate and phosphate from fossil tooth enamel. *Geochimica et Cosmochimica Acta*, *68*(10), 2245–2258. https://doi.org/10.1016/j.gca.2003.11.009

Zheng, D., Hunt, E. R. Jr., & Running, S. W. (1993). A daily soil temperature model based on air temperature and precipitation for continental applications. *Climate Research*, *2*(3), 183–191. https://doi.org/10.3354/cr002183